Mathematical Biosciences and Engineering

https://www.aimspress.com/journal/mbe

MBE, 23(8): 2228–2258.
DOI: 10.3934/mbe.2026081
Received: 28 April 2026
Revised: 08 June 2026
Accepted: 07 July 2026
Published: 21 July 2026

Research article

Quantification of various types of uncertainty in biological computational models using fuzzy mass functions

Isai Chavarri[1], Yanyan He[2,*], Minyi Chen[1], John W. Cain[3] and Lindsay Waldrop[4]

[1] Department of Mathematics, University of North Texas, 1155 Union Circle, Denton 76203, TX, USA
[2] Department of Mathematics, and of Computer Science and Engineering, University of North Texas, 1155 Union Circle, Denton 76203, TX, USA
[3] Department of Mathematics, Harvard University, One Oxford Street, Cambridge 02138, MA, USA
[4] Schmid College of Science and Technology, Chapman University, One University Drive, Orange 92866, CA, USA

* **Correspondence:** Email: yanyan.he@unt.edu.

Abstract: We develop a unified uncertainty propagation framework for computational models involving stochastic variability together with two distinct forms of epistemic uncertainty: vagueness and incomplete knowledge. In this framework, stochastic uncertainty is represented by random variables, while the epistemic components are modeled by random fuzzy sets with fuzzy mass functions generalized from Dempster-Shafer theory and fuzzy set theory. Using generalized polynomial chaos expansions and extension principles, the propagated uncertainty in output expectation is then quantified efficiently by a fuzzy mass function. We also introduce a distance measure between fuzzy mass functions and use it to analyze the error in the resulting numerical approximations. The proposed approach is demonstrated on several simple examples and applied to two biological systems: the Mitchell-Schaeffer model governed by a system of ordinary differential equations, and a computational model of olfaction governed by the Navier-Stokes equations.

Keywords: fuzzy sets; fuzzy mass function; generalized polynomial chaos; Dempster-Shafer theory; Mitchell-Schaeffer model; olfaction

1. Introduction

It is increasingly recognized that multiple forms of uncertainty affect the modeling and simulation process of physical systems [1–5]. Some model parameters vary because of inherent randomness, some are uncertain because the available data are limited, and some are specified imprecisely because the available information lacks clarity. Therefore, a comprehensive uncertainty quantification (UQ) framework is needed to represent, propagate, and analyze the different types of uncertainty that may coexist within the same physical system.

Probability theory, through random variables and probability density functions, provides a natural framework for describing aleatory variability. However, it may not be suitable for addressing epistemic uncertainty – uncertainty due to lack of knowledge or clarity [6]. To tackle epistemic UQ, it is important to consider alternative mathematical frameworks. For example, fuzzy set theory uses membership functions to capture the graded and vague nature of imprecise descriptions [7, 8], while Dempster-Shafer (DS) theory relaxes the additivity constraint of probability measures by assigning belief mass to sets rather than points, making it well-suited for representing uncertainty due to lack of knowledge [9–11]. There are other related frameworks such as possibility theory [12, 13], generalized p-boxes [14], and interval analysis.

Several researchers have focused on individual theories for specific types of uncertainty. In purely probabilistic settings, methods such as the Monte Carlo method and generalized polynomial chaos (gPC) expansion [15–19] have been widely used to quantify stochastic uncertainty arising from randomness. For epistemic uncertainty caused by incomplete knowledge, DS-theory-based UQ methods have been developed and adopted in a variety of applications [20–24]. For epistemic uncertainty due to lack of clarity, fuzzy-set-based propagation methods have also been studied extensively in engineering and scientific applications [25–28].

Pairwise combinations of these theories have also been used to develop mixed-UQ approaches. For example, in previous work, we combined DS theory with the gPC method to quantify both epistemic and aleatory uncertainties in synthetic problems [20]. Fuzzy set theory has been combined separately with DS theory or probability theory in reliability analysis and engineering systems [29, 30]. These hybrid UQ approaches have proven effective for both benchmark examples and practical problems. However, research on a mixed-UQ framework that combines probability theory, fuzzy set theory, and DS theory (which is capable of addressing randomness, vagueness, and partial knowledge coexisting in the same system) remains very limited. Additionally, to the best of our knowledge, no rigorous error analysis is currently available for efficient mixed-UQ methods built upon the combination of these three theories.

To address this gap, we propose a unified numerical UQ framework that jointly propagates aleatory uncertainty and two distinct types of epistemic uncertainty through a single simulation model. First, under the assumption of independence among all uncertain inputs, we construct fuzzy mass functions for random fuzzy sets [31, 32] based on fuzzy set theory and DS theory, to represent two forms of epistemic uncertainty in the inputs. Second, we propagate the mixed uncertainty using gPC expansion coupled with extension principles [33–36], and obtain fuzzy mass functions to represent uncertainty in output expectation. Third, we introduce a new distance measure between two fuzzy mass functions, leveraging the concepts of Hausdorff distance [20, 37], and use it to conduct a rigorous error analysis of the proposed method. Finally, we demonstrate the approach on several examples involving both ordinary differential equations (ODEs) and partial differential equations (PDEs). The main contributions of this work include the development of a numerical algorithm for propagating fuzzy mass functions, the error analysis for mixed uncertainty propagation when gPC expansions are used as approximations over stochastic space, and the novel application of the proposed methodology to biological computational models.

The paper is organized as follows. In Section 2, we present the relevant concepts from fuzzy set theory and DS theory, introduce random fuzzy sets with fuzzy mass functions, and define a distance metric between two fuzzy mass functions. In Section 3, we describe the comprehensive numerical method for propagating mixed stochastic and various epistemic uncertainties, together with its error analysis. The method is demonstrated on several illustrative examples in Section 4. In Section 5, we apply the approach to two biological models governed by differential systems. Finally, we conclude the paper with a summary and conclusion in Section 6.

2. Preliminaries

In this section, we introduce the basic concepts from fuzzy set theory, DS theory, and random fuzzy sets.

2.1. Basics of fuzzy set theory

Let x be an element of a nonempty classical set X. A fuzzy set $\widetilde{A} \subset X$ is defined as the collection of ordered pairs:

$$\widetilde{A} = \{(x, \mu_{\widetilde{A}}(x))|x \in X\},$$

where $\mu_{\widetilde{A}}(x) : X \to [0,1]$ (or simply $\widetilde{A}(x)$) is called the *membership function*. The value $\mu_{\widetilde{A}}(x)$ represents the degree of membership of x in the fuzzy set $\widetilde{A}$.

The set of elements that belong to $\widetilde{A}$ with membership degree at least α, i.e.,

$$\{x \in X|\widetilde{A}(x) \geq \alpha\},$$

is called the α-cut, denoted as $[\widetilde{A}]_\alpha$. The corresponding strong α-cut, denoted as $[\widetilde{A}]_{\alpha^+}$, is defined with strict inequality. The *support* of $\widetilde{A}$ is the set of all elements with nonzero membership, denoted as $supp(\widetilde{A})$. All three are crisp sets that characterize $\widetilde{A}$. A fuzzy set $\widetilde{A}$ is called *normal* if $\sup \mu_{\widetilde{A}}(x) = 1$.

The basic operations on fuzzy sets were introduced by Zadeh [7]. Specifically, the membership functions of the intersection and union of two fuzzy sets $\widetilde{A}$ and $\widetilde{B}$ are defined as follows, respectively:

$$\begin{aligned} \mu_{\widetilde{A}\cap\widetilde{B}}(x) &= \min(\mu_{\widetilde{A}}(x), \mu_{\widetilde{B}}(x)), x \in X; \\ \mu_{\widetilde{A}\cup\widetilde{B}}(x) &= \max(\mu_{\widetilde{A}}(x), \mu_{\widetilde{B}}(x)), x \in X. \end{aligned} \tag{1}$$

Zadeh's extension principle provides a standard way to define functions over fuzzy sets. We state it in a general form [35, 36].

Definition 1 (Zadeh's extension principle). Let $\widetilde{A}_1, \ldots, \widetilde{A}_{n_\Xi}$ be fuzzy sets with corresponding membership functions $\mu_{\widetilde{A}_1}, \ldots, \mu_{\widetilde{A}_{n_\Xi}}$ defined on $X_1, \ldots, X_{n_\Xi}$, respectively, and let X be a Cartesian product $X = X_1 \times \cdots \times X_{n_\Xi}$. Let f be a mapping from X to a set U, i.e., $u = f(x_1, x_2, ..., x_{n_\Xi})$. Then, the extension principle defines a fuzzy set $\widetilde{B}$ in U by

$$\widetilde{B} = \{(u, \mu_{\widetilde{B}}(u))|u = f(x_1, \ldots, x_{n_\Xi}), (x_1, \ldots, x_{n_\Xi}) \in X\}, \tag{2}$$

where

$$\mu_{\widetilde{B}}(u) = \begin{cases} \sup_{(x_1,\ldots,x_{n_\Xi})\in f^{-1}(u)} \min\{\mu_{\widetilde{A}_1}(x_1), \ldots, \mu_{\widetilde{A}_{n_\Xi}}(x_{n_\Xi})\}, & \text{if } f^{-1}(u) \neq \emptyset, \\ 0, & \text{otherwise,} \end{cases} \tag{3}$$

where f^{-1} is the inverse of f.

2.2. Basics of DS theory

Assume that the collected evidence, regarding the quantity of interest $\zeta \in Z$, can be interpreted in finitely many ways with given probabilities [9,31]. If the interpretation $\omega \in \Omega$ (where Ω is the finite set of all interpretations) holds, then the evidence indicates that the proposition "the true value of ζ falls in $\Gamma(\omega) \subseteq Z$ " is true, with no further specification, where Γ is a mapping from Ω to 2^Z. We further assume that a probability measure P can be defined on $(\Omega, 2^\Omega)$. Then the tuple $(\Omega, 2^\Omega, P, \Gamma)$ is a random set. The corresponding *mass function* $m : 2^Z \to [0, 1]$ is defined as in [31].

$$m(A) = P(\omega \in \Omega : \Gamma(\omega) = A), \tag{4}$$

for all nonempty subsets $A \subseteq Z$, with $m(\emptyset) = 0$. A subset A is called a focal element of m if $m(A)$ is nonzero. The mass function is also called the basic belief assignment (BBA) or m-function in [9,10,34,38,39] (hereafter, we use mass function and m-function interchangeably).

Using the mass function, the belief and plausibility functions are defined as

$$Bel(A) = \sum_{B \subseteq A} m(B), \qquad Pl(A) = \sum_{B \cap A \neq \emptyset} m(B). \tag{5}$$

The belief function measures the expected necessity of the proposition $\zeta \in A$, indicating the total support from the evidence on A (including all subsets of A); while the plausibility function measures the expected possibility of the proposition, indicating the maximum possible strength of the evidence supporting $\zeta \in A$. These two functions are linked by the duality relation $Pl(A) = 1 - Bel(\overline{A})$.

The cumulative belief function (CBF) and cumulative plausibility function (CPF) of a belief function in DS theory are defined as follows [6,40]:

$$\begin{aligned} CBF(z) &= Bel(\zeta \in (-\infty, z]), & (6)\\ CPF(z) &= Pl(\zeta \in (-\infty, z]). & (7) \end{aligned}$$

The extension principle in the framework of DS theory has been defined as in [33,41].

Definition 2. Let $u = f(\zeta)$ be a mapping from the domain $Z \subset \mathcal{R}^{nz}$ to a domain U, and let m_ζ be the mass function associated with the variable ζ, with focal elements $A_1, A_2, \ldots, A_{\hat{n}}$. Then the mass function m_u of the output u is defined for any $B \subset U$ as the following

$$m_u(B) = \begin{cases} \sum_{i \in I} m_\zeta(A_i), & \text{if } I = \{i | f(A_i) = B\} \text{ is nonempty,} \\ 0, & \text{otherwise.} \end{cases} \tag{8}$$

2.3. Fuzzy mass functions

To handle evidence that is both uncertain and fuzzy, DS theory is generalized, and random fuzzy sets and fuzzy mass functions are defined [31,32]. Consider a quantity $\theta \in \Theta$, and let $\mathcal{F}^*(\Theta)$ be the set of all normal fuzzy subsets of Θ. As in Section 2.2, we assume that the evidence can be interpreted in a finite number of different ways, and the finite set of all interpretations is denoted as Ω. If the interpretation $\omega \in \Omega$ holds, then the proposition "the true value of $\theta \in \Theta$ falls in $\widetilde{\Gamma}(\omega) \subseteq \Theta$ " is true, and nothing more, where $\widetilde{\Gamma} : \Omega \to \mathcal{F}^*(\Theta)$ maps each interpretation to a normal fuzzy subset of Θ. As before, we further assume the existence of a probability measure P on $(\Omega, 2^{\Omega})$. Then the tuple $(\Omega, 2^{\Omega}, P, \widetilde{\Gamma})$ is a random fuzzy set [31,42]. The corresponding fuzzy mass function $m : \mathcal{F}^*(\Theta) \to [0,1]$ is defined as

$$\widetilde{m}(\widetilde{A}) = P(\omega \in \Omega : \widetilde{\Gamma}(\omega) = \widetilde{A}). \tag{9}$$

The set $\widetilde{A}$ is called a (fuzzy) focal element of $\widetilde{m}$ if $\widetilde{m}(\widetilde{A}) > 0$. Note that the number of focal elements is finite due to the assumption of Ω being finite. The quantity $\widetilde{m}(\widetilde{A})$ indicates the strength of the evidence that supports the proposition "θ is in $\widetilde{A}$", without supporting any more specific propositions.

Let $\widetilde{A}_1, \ldots, \widetilde{A}_{\widetilde{n}}$ denote all the focal elements, and the plausibility and belief of a crisp set A are defined in [31,43]

$$Pl_{\widetilde{m}}(A) = \sum_{i=1}^{\widetilde{n}} \widetilde{m}(\widetilde{A}_i) \max_{z \in A} \widetilde{A}_i(z), \tag{10}$$

$$Bel_{\widetilde{m}}(A) = \sum_{i=1}^{\widetilde{n}} \widetilde{m}(\widetilde{A}_i) \min_{z \notin A} [1 - \widetilde{A}_i(z)]. \tag{11}$$

2.4. Distance between two fuzzy mass functions

For the purpose of error analysis, we introduce a distance to measure the difference between the numerical approximation fuzzy mass function obtained from a numerical algorithm and the true one. Before that, let us first recall the distance between two fuzzy sets and its properties introduced in [37].

Definition 3. Let $\widetilde{A}$ be a fuzzy set defined on X, f and g be two mappings on X, and $\widetilde{F} = f(\widetilde{A})$ and $\widetilde{G} = g(\widetilde{A})$ be the corresponding fuzzy sets defined by Definition 1. For $\alpha \in [0,1]$, let $\widetilde{F}_{\alpha^+} = f([\widetilde{A}]_{\alpha^+})$ and $\widetilde{G}_{\alpha^+} = g([\widetilde{A}]_{\alpha^+})$.Then the distance between two fuzzy sets $\widetilde{F}$ and $\widetilde{G}$ is defined as, for $p \geq 1$ [37]

$$D^p(\widetilde{F}, \widetilde{G}) = \int_0^1 d_{H^p}(\widetilde{F}_{\alpha^+}, \widetilde{G}_{\alpha^+}) d\alpha, \tag{12}$$

where

$$\begin{aligned} d_{H^p}(\widetilde{F}_{\alpha^+}, \widetilde{G}_{\alpha^+}) = \max\{ & (\int_{s \in [\widetilde{A}]_{\alpha^+}} \operatorname{essinf}_{r \in [\widetilde{A}]_{\alpha^+}} d^p(f(s), g(r)) ds))^{1/p}, \\ & (\int_{r \in [\widetilde{A}]_{\alpha^+}} \operatorname{essinf}_{s \in [\widetilde{A}]_{\alpha^+}} d^p(f(s), g(r)) dr))^{1/p} \}, \end{aligned} \tag{13}$$

and d represents the classical distance between two elements.

Note that d_{H^p} distance with $p = 1$ is a relaxed version of the well-known Hausdorff distance [37]. That is for any two classical nonempty sets A, B, we have

$$d_H(A, B) = \max\{\sup_{s \in A} \inf_{r \in B} d(s, r), \sup_{r \in B} \inf_{s \in A} d(s, r)\}.$$

Theorem 2.1. *Following Definition 3 with $d(x, y) = |x - y|$, and with $S = supp(\widetilde{A})$, for any $\alpha \in [0,1]$, we have [37]*

$$d_{H^p}(\widetilde{F}_{\alpha^+}, \widetilde{G}_{\alpha^+}) \leq \|f - g\|_{\mathcal{L}^p(S)}. \tag{14}$$

We then recall the distance between two mass functions defined in [20].

Definition 4. Let $\theta \in \Theta$ be the input parameter associated with a mass function m_θ. Let A_i $(1 \leq i \leq \hat{n})$ be the focal elements with belief masses $m_\theta(A_i)$. Consider two mappings f, g on Θ and the mass functions m_f, m_g for the corresponding outputs defined by Definition 2. Let $F_i = f(A_i)$ and $G_i = g(A_i)$. Then the distance between the two mass functions m_f and m_g is

$$D^p(m_f, m_g) = \sum_{i=1}^{\hat{n}} m_\theta(A_i) d_{H^p}(F_i, G_i). \tag{15}$$

Hausdorff distance d_H is used in [20] with p=1. Next, we extend Definition 2 to the extension principle for fuzzy mass functions and extend the Definitions 3 and 4 to a distance measure between two fuzzy mass functions.

Definition 5. Let $u = f(\theta)$ be a mapping from the domain $\Theta \subset \mathcal{R}^{nz}$ to a domain U, and let $\widetilde{m}_\theta$ be the fuzzy mass function associated with the variable θ, where its focal elements are a finite number of fuzzy sets $\{\widetilde{A}_1, \widetilde{A}_2, \ldots, \widetilde{A}_{\widetilde{n}}\}$. Let $\mathcal{F}^*(U)$ denote the collection of all normal fuzzy sets of U. Then the fuzzy mass function $\widetilde{m}_u$ of the output function u, is defined for any $\widetilde{B} \in \mathcal{F}^*(U)$ as the following

$$\widetilde{m}_u(\widetilde{B}) = \begin{cases} \sum_{i \in I} \widetilde{m}_\theta(\widetilde{A}_i), & \text{if } I = \{i | f(\widetilde{A}_i) = \widetilde{B}\} \text{ is nonempty,} \\ 0, & \text{otherwise,} \end{cases} \tag{16}$$

where $f(\widetilde{A}_i)$ is the corresponding fuzzy sets defined by Definition 1.

We finally define the distance between two fuzzy mass functions.

Definition 6. Let $\theta \in \Theta$ be an input variable associated with a fuzzy mass function $\widetilde{m}_\theta$, which has a finite number of focal elements $\widetilde{A}_i$ $(1 \leq i \leq \widetilde{n})$ with the corresponding belief masses $\widetilde{m}(\widetilde{A}_i)$. Consider two mappings f, g on Θ and the fuzzy mass functions $\widetilde{m}_f, \widetilde{m}_g$ for the corresponding outputs defined by Definition 5. Let $\widetilde{F}_i = f(\widetilde{A}_i)$ and $\widetilde{G}_i = g(\widetilde{A}_i)$. Then the distance between the two fuzzy mass functions $\widetilde{m}_f$ and $\widetilde{m}_g$ is

$$\widetilde{D}^p(\widetilde{m}_f, \widetilde{m}_g) = \sum_{i=1}^{\widetilde{n}} \widetilde{m}_\theta(\widetilde{A}_i) D^p(\widetilde{F}_i, \widetilde{G}_i). \tag{17}$$

This satisfies the following properties:

- $\widetilde{D}^p(\widetilde{m}_f, \widetilde{m}_g) \geq 0$ and $\widetilde{D}^p(\widetilde{m}_f, \widetilde{m}_g) = 0 \implies \widetilde{m}_f = \widetilde{m}_g$.
- $\widetilde{D}^p(\widetilde{m}_f, \widetilde{m}_g) = \widetilde{D}^p(\widetilde{m}_g, \widetilde{m}_f)$.
- $\widetilde{D}^p(\widetilde{m}_f, \widetilde{m}_g) \leq \widetilde{D}^p(\widetilde{m}_f, \widetilde{m}_h) + \widetilde{D}^p(\widetilde{m}_h, \widetilde{m}_g)$, where $\widetilde{m}_h$ is the fuzzy mass function for the output of function $h(\theta)$.

Theorem 2.2. *Let $\widetilde{D}^p(\widetilde{m}_f, \widetilde{m}_g)$ be the distance defined in Definition 6. Denote $S_i = supp(\widetilde{A}_i)$. If $\|f - g\|_{L^p(S_i)} \leq \epsilon$ for all $1 \leq i \leq \widetilde{n}$, we have*

$$\widetilde{D}^p(\widetilde{m}_f, \widetilde{m}_g) \leq \epsilon. \tag{18}$$

Proof: Observe

$$\widetilde{D}^p(\widetilde{m}_f, \widetilde{m}_g) = \sum_{i=1}^{\widetilde{n}} \widetilde{m}_\theta(\widetilde{A}_i) D^p(\widetilde{F}_i, \widetilde{G}_i).$$

According to Eq (14) and the assumption, we have

$$d_{H^p}(\widetilde{F}_{i,\alpha^+}, \widetilde{G}_{i,\alpha^+}) \leq \|f - g\|_{L^p(S_i)} \leq \epsilon.$$

With Eq (12),

$$\begin{aligned} D^p(\widetilde{F}_i, \widetilde{G}_i) &= \int_0^1 d_{H^p}(\widetilde{F}_{i,\alpha^+}, \widetilde{G}_{i,\alpha^+}) d\alpha, \\ &\leq \epsilon \int_0^1 d\alpha = \epsilon. \end{aligned} \tag{19}$$

Following that, we have

$$\widetilde{D}^p(\widetilde{m}_f, \widetilde{m}_g) = \sum_{i=1}^{\widetilde{n}} \widetilde{m}_\theta(\widetilde{A}_i) D^p(\widetilde{F}_i, \widetilde{G}_i) \leq \sum_{i=1}^{\widetilde{n}} \widetilde{m}_\theta(\widetilde{A}_i)\epsilon \leq \epsilon.$$

Table 1 summarizes the key notation introduced in this section and used throughout the paper.

Table 1. Notation summary.

ξ	fuzzy variables
ζ	DS uncertain variables
y, $\eta(y)$	random variables and their PDF
$\widetilde{A}$, $\mu_{\widetilde{A}}$	fuzzy set and its membership function
$[\widetilde{A}]_\alpha$, supp$(\widetilde{A})$	α-cut and support
$\widetilde{\Xi A_i}$	fuzzy set from $\widetilde{\Xi}$ paired with crisp A_i
m_ζ, A_i	mass function and crisp focal elements
$\widetilde{m}$, $\widetilde{A}_i$	fuzzy mass function and fuzzy focal elements
Bel, Pl, CBF, CPF	belief, plausibility, cumulative belief and plausibility functions
$u(\xi, \zeta, y)$	model output
$E(\xi, \zeta)$, $E_n(\xi, \zeta)$	true and gPC-approximated conditional expectation
$\widetilde{B}_i$, $\widetilde{B}_{n,i}$	output fuzzy focal elements (true / from gPC)
$\widetilde{m}_E$, $\widetilde{m}_{E_n}$	output fuzzy mass functions for E and E_n
$D^p(\widetilde{F}, \widetilde{G})$	distance between two fuzzy sets
$D^p(m_f, m_g)$	distance between two mass functions
$\widetilde{D}^p(\widetilde{m}_f, \widetilde{m}_g)$	distance between two fuzzy mass functions

3. Uncertainty propagation using fuzzy set and DS theories

In this section, we present a numerical strategy for uncertainty propagation in a general computational model governed by a differential equation on a spatial domain D and a time interval $(0, T]$. The various types of uncertainty in the system are represented using three types of uncertain variables: (i) fuzzy variables $\xi = \{\xi_1, \ldots, \xi_{n_\Xi}\} \in \Xi \subset \mathcal{R}^{n_\Xi}$ representing epistemic uncertainty due to vagueness or lack of clarity; (ii) uncertain variables $\zeta = \{\zeta_1, \ldots, \zeta_{n_Z}\} \in Z \subset \mathcal{R}^{n_Z}$ representing epistemic uncertainty stemming from lack of knowledge; and (iii) random variables $y = \{y_1, y_2, \ldots, y_{n_Y}\} \in Y \subset \mathcal{R}^{n_Y}$ representing aleatory uncertainty from randomness in the system.

The mathematical model is assumed to be well-posed in $Y \times \Xi \times Z$, and the model output ($u(x, t, y, \xi, \zeta)$ or a function of u) is assumed to be continuous over the domain $\Xi \times Z$. Given membership functions for ξ, mass functions in DS theory for ζ, and probability density functions for y, the objective of uncertainty propagation is to quantify the uncertainty in the model output propagated from the mixed aleatory and epistemic uncertainty in the input variables. Without loss of generality, we consider scalar model output (i.e., $u \in \mathcal{R}$). For simplicity in notation, we omit the dependence of the solution on the variables x and t, and focus on the problem for any fixed $x \in D$ and $t \in (0, T]$. Accordingly, the output is denoted as $u(\xi, \zeta, y)$. This approach is standard in most of the uncertainty quantification (UQ) literature [37].

3.1. Epistemic uncertainty propagation

We first consider the epistemic uncertainty in the system, characterized by the non-probabilistic uncertain variables $\xi \in \widetilde{\Xi}$ with membership function $\mu_{\widetilde{\Xi}}(\xi)$ (and its support is denoted as Ξ) and $\zeta \in Z$ with mass function m_ζ (with focal elements A_i, $i = 1, \ldots, \hat{n}$).

Consider A_i to be a fuzzy set with membership function $\mu_{A_i}(\zeta) = 1$ for $\zeta \in A_i$ and $\mu_{A_i}(\zeta) = 0$ for $\zeta \notin A_i$. The 2D fuzzy set $\widetilde{\Xi A_i} = \{(\xi, \zeta), \mu_{\widetilde{\Xi A_i}}(\xi, \zeta)\}$ has membership function as

$$\mu_{\widetilde{\Xi A_i}}(\xi, \zeta) = \min(\mu_{\widetilde{\Xi}}(\xi), \mu_{A_i}(\zeta)) = \mu_{\widetilde{\Xi}}(\xi). \tag{20}$$

Then a fuzzy mass function can be defined with the fuzzy focal elements $\widetilde{\Xi A_i}$ (for $i = 1, \ldots, \hat{n}$)

$$\widetilde{m}(\widetilde{\Xi A_i}) = P((\xi, \zeta) \in \widetilde{\Xi A_i}) = P(\xi \in \widetilde{\Xi})P(\zeta \in A_i) = P(\zeta \in A_i) = m_\zeta(A_i). \tag{21}$$

The quantity $\widetilde{m}(\widetilde{\Xi A_i})$ is interpreted as the degree to which the evidence supports the proposition "(ξ, ζ) falls inside the fuzzy set $\widetilde{\Xi A_i}$".

We now propagate the epistemic uncertainty in (ξ, ζ) represented by the fuzzy mass function through the system, and represent the uncertainty in the output $u(\xi, \zeta)$ by a fuzzy mass function using Definition 5. Numerically, for each input fuzzy focal element $\widetilde{\Xi A_i}$, the corresponding output fuzzy focal element $\widetilde{B}_i$ can be obtained using the extension principle for fuzzy sets. Specifically, we characterize the input fuzzy set by a finite number of α-cut. For each α-cut of $\widetilde{\Xi A_i}$ (which is a classical set), one pair of optimizations can be implemented

$$B_{i,\alpha,1} = \min_{\{\xi,\zeta\} \in [\widetilde{\Xi A_i}]_\alpha} u(\xi, \zeta), \tag{22}$$

$$B_{i,\alpha,2} = \max_{\{\xi,\zeta\} \in [\widetilde{\Xi A_i}]_\alpha} u(\xi, \zeta). \tag{23}$$

The interval $[B_{i,\alpha,1}, B_{i,\alpha,2}]$ serves as the corresponding α-cut of the output fuzzy set $\widetilde{B}_i$. The resulting $\widetilde{B}_i$ then becomes a fuzzy focal element of the output u, and its belief mass $\widetilde{m}(\widetilde{B}_i)$ is the same as $\widetilde{m}(\widetilde{\Xi \mathcal{A}_i})$, which is also the same as $m_\zeta(A_i)$. The output fuzzy mass function has the same number of fuzzy focal elements as the input, unless more than one input fuzzy set is mapped to the same fuzzy focal element. Note: Since optimization is not the primary focus of this work, we employ a simple and easy-to-implement sampling strategy to solve the optimization problems. This approach provides an approximation of the global optimum. While this deterministic sampling method is sufficient for this study, the computational efficiency and accuracy of the optimization could potentially be improved by using alternative optimization techniques, such as multi-start local optimization methods or global optimization algorithms, including efficient global optimization.

3.2. Mixed aleatory and epistemic uncertainty propagation

Whereas epistemic uncertainty is represented using fuzzy mass functions, the mixed uncertainty propagation problem also involves the aleatory uncertainty characterized by the random variable $y \in Y$ with probability density function denoted as $\eta(y)$. The mixed types of uncertainty are propagated through the system, and the goal is to mathematically represent the uncertainty in the output $u(\xi, \zeta, y) : \Xi \times Z \times Y \to U$. With the probability density function for the random variable y, one can evaluate the statistics of output u over the space Y, such as its expectation

$$E(\xi, \zeta) = E[u(\xi, \zeta, y)|\xi, \zeta] = \int_Y u(\xi, \zeta, y)\eta(y)dy, \qquad \xi \in \Xi, \zeta \in Z. \tag{24}$$

Because of the mixed types of uncertainty, the expectation $E(\xi, \zeta)$ is not deterministic; rather, it is a function of the non-probabilistic variables ξ and ζ. Since fuzzy sets and belief functions represent the uncertain information associated with the input variables ξ, ζ, the goal then becomes to obtain a fuzzy mass function for the expectation of the model output u (i.e., obtain $\widetilde{m}_E$) using the epistemic UQ method described in Section 3.1. For the purpose of efficiency, we employ the gPC method to construct the computationally cheaper surrogate $E_n(\xi, \zeta)$ that approximates the truth $E(\xi, \zeta)$, where n is the approximation polynomial order.

3.3. Generalized polynomial chaos method

Here, we provide the basics of the gPC method. Any second-order random variable $u(y(\omega)) \in \mathbf{L}_2(\Omega, \mathcal{P})$ can be approximated using the following gPC expansion [16, 44–46]:

$$u_n(y(\omega)) = \sum_{i=0}^{N-1} u_i \Phi_i(y(\omega)), \tag{25}$$

where Ω is the sample space and $\omega \in \Omega$, $\mathcal{P} : 2^{\Omega} \to [0, 1]$ is the probability measure, n is the highest polynomial order, $N = (n_Y + n)!/(n_Y!n!)$ is the number of terms, and u_is are the gPC coefficients to be determined. The functions Φ_i are generalized polynomial chaos (e.g., Wiener-Hermite polynomial chaos or Legendre polynomial chaos) [15, 16]. By choosing the proper type of polynomial chaos (matching the weighting function of these orthogonal polynomials to the probability density function), the gPC expansion can achieve rapid convergence to smooth functions.

To obtain the values for gPC coefficients, the orthogonality of the polynomial basis enables us to project u onto each basis function with the inner product

$$u_i = \frac{< u, \Phi_i >}{< \Phi_i, \Phi_i >} = \frac{1}{E[\Phi_i^2]} \int_Y u(y)\Phi_i(y)\eta(y)dy. \tag{26}$$

Numerically, the integration can be approximated using a quadrature rule with data $u(y^{(j)})$ at a set of quadrature points $\{y^{(j)}\}_{j=1}^{M}$ as

$$u_i \approx \hat{u}_i = \frac{1}{E[\Phi_i^2]} \sum_{j=1}^{M} u(y^{(j)})\Phi_i(y^{(j)})w^{(j)}, \qquad i = 0, 1, \ldots, N-1, \tag{27}$$

where $\{w^{(j)}\}_{j=1}^{M}$ are the corresponding weights. To reduce the computational cost for high-dimensional problems, sparse-grid quadrature can be considered for gPC construction [47].

The projection method (Galerkin projection) yields the best approximation in the weighted $L_2(\eta)$ norm [46], where η is typically taken as the tensor product of the input marginals, and the multivariate polynomial basis is constructed as the product of univariate polynomials. When the random variables are dependent, the assumed product measure deviates from the true joint distribution, and the resulting surrogate may not minimize the L_2 error under that distribution. Alternatively, the gPC coefficients can be estimated by solving a Least Squares problem on a dataset $\{y^{(j)}, u(y^{(j)})\}_{j=1}^{M}$. The Least Squares problem for the solution $\hat{\boldsymbol{u}} = [\hat{u}_0, \hat{u}_1, \ldots, \hat{u}_{N-1}]$ is stated as

$$\hat{\boldsymbol{u}} = \arg\min_{\boldsymbol{u}} \left\| \sum_{i=0}^{N-1} u_i \Phi_i(\boldsymbol{y}) - u(\boldsymbol{y}) \right\|_2, \tag{28}$$

where $\boldsymbol{y} = \{y^{(j)}\}$, and $\boldsymbol{u} = [u_0, u_1, \ldots, u_{N-1}]$ denotes an arbitrary gPC coefficient vector that converges to the desired coefficient vector $\hat{\boldsymbol{u}}$ through the minimization.

With the numerical approximation $u_n(y)$, one can obtain an approximation E_n to the expectation. Including the uncertain non-probabilistic variables ξ, ζ, the truncated gPC expansion u_n and its expectation E_n are updated as

$$u_n(\xi, \zeta, y) = \sum_{i=0}^{N-1} u_i(\xi, \zeta)\Phi_i(y), \tag{29}$$

$$E_n(\xi, \zeta) = \int_Y u_n(\xi, \zeta, y)\eta(y)dy. \tag{30}$$

As mentioned in Section 3.1, the epistemic uncertainty in the approximated expectation $E_n(\xi, \zeta)$ is represented using a fuzzy mass function $\widetilde{m}_{E_n}$.

The error in the obtained fuzzy mass function $\widetilde{m}_{E_n}$ can be quantified using the distance defined in Section 2.4.

Theorem 3.1. *Let $E(\xi, \zeta)$ and $E_n(\xi, \zeta)$ be the true expectation and its approximation defined as in Eqs (24) and (30), respectively. Recall that $\xi \in \widetilde{\Xi}$ is associated with membership function $\mu_{\widetilde{\Xi}}(\xi)$, and ζ is associated with a mass function m_ζ with a finite number of focal elements $\{A_i\}_{i=1}^{\hat{n}}$. Denote the fuzzy mass function of $E(\xi, \zeta)$ by $\widetilde{m}_E$ with fuzzy focal elements $\widetilde{B}_i$s, and the fuzzy mass function of $E_n(\xi, \zeta)$ by $\widetilde{m}_{E_n}$ with fuzzy focal elements $\widetilde{B}_{n,i}$s obtained by the proposed method. If $\|u(y, \xi, \zeta) - u_n(y, \xi, \zeta)\|_{L_\eta^p(Y)} \leq \epsilon_n$ for all $(\xi, \zeta) \in \Xi \times Z$ and the assumption that u is continuous over $\Xi \times Z$, then we have*

$$|\widetilde{D}^p(\widetilde{m}_E, \widetilde{m}_{E_n})| \leq \epsilon_n. \tag{31}$$

Proof: Since for all $\{\xi, \zeta\} \in \Xi \times Z$, $\|u(y, \xi, \zeta) - u_n(y, \xi, \zeta)\|_{L^p_\eta(Y)} \leq \epsilon_n$, one can easily show that the error in the approximation E_n is bounded by the error in the approximation u_n for any $\{\xi, \zeta\} \in \Xi \times Z$, and consequently, we have $|E(\xi, \zeta) - E_n(\xi, \zeta)|_{L^p(\Xi \times A_i)} \leq \epsilon_n$ for all i.

Since u and u_n are continuous over $\Xi \times Z$, their expectations $E(\xi, \zeta)$ and $E_n(\xi, \zeta)$ are continuous over $\Xi \times Z$ as well. In addition, all the α-cuts of the fuzzy focal elements of the output fuzzy mass function are continuous domains.

Since $\widetilde{D}^p(\widetilde{m}_E, \widetilde{m}_{E_n}) = \sum_i m_\zeta(A_i) D^p(\widetilde{B}_i, \widetilde{B}_{n,i})$, using Theorem 2.2, one can conclude that Eq (31) holds.

Algorithm 1 : **Evaluation of $E_n(\xi, \zeta)$ (with fixed ξ, ζ) via gPC**

Input: Random variables $y \in Y \subset \mathcal{R}^{n_Y}$ with $\eta(y)$; Function u

Specify a set of points $\{y^{(j)}\}_{j=1}^M$ (or quadrature points$\{y^{(j)}, w^{(j)}\}_{j=1}^M$ for projection)
Solve the differential equation at chosen points to obtain $u(\xi, \zeta, y^{(j)})$
Compute gPC expansion as in Section 3.3, obtain $u_n(\xi, \zeta, y)$
Evaluate $E_n(\xi, \zeta)$ using Eq (30).

Algorithm 2 : **Propagation of epistemic uncertainty: output fuzzy mass function**

Input
Fuzzy variables $\xi_j \in \widetilde{\Xi}_j$ with $\mu_{\widetilde{\Xi}_j}$, $j = 1, \ldots, n_\Xi$; Function E_n
Uncertain variables $\zeta_i \in Z_i$ with m_{ζ_i}: focal elements A_{i,k_i}, $i = 1, \ldots, n_Z$

Obtain a single fuzzy set $\widetilde{\Xi}$
Obtain $\widetilde{\Xi} = \{\xi, \mu_{\widetilde{\Xi}}(\xi)\}$, where $\xi = \{\xi_1, \ldots, \xi_{n_\Xi}\}$.
Membership function $\mu_{\widetilde{\Xi}}(\xi_1, \ldots, \xi_{n_\Xi}) = \min(\mu_{\widetilde{\Xi}_1}(\xi_1), \ldots, \mu_{\widetilde{\Xi}_{n_\Xi}}(\xi_{n_\Xi}))$

Obtain a single mass function m_ζ
Obtain n_Z-dimensional hypercube $A_k = A_{1,k_1} \times \ldots \times A_{n_Z,k_{n_Z}}$
Belief mass $m_\zeta(A_k) = \Pi_{i=1}^{n_Z} m_{\zeta_i}(A_{ik_i})$

Input fuzzy mass function
Fuzzy focal element $\widetilde{\Xi A_i}$ with membership function in Eq (20)
Fuzzy belief mass $\widetilde{m}(\widetilde{\Xi A_i})$ defined in Eq (21)

Obtain output fuzzy mass function $\widetilde{m}_{E_n}$
for all fuzzy focal elements $\widetilde{\Xi A_i}$ **do**
  Obtain the corresponding fuzzy focal element $\widetilde{B}_i$ of $\widetilde{m}_{E_n}$
  for $\alpha \in [0, 1]$ **do**
    Consider $[\widetilde{\Xi A_i}]_\alpha = \{(\xi, \zeta) \in \Xi \times Z | \mu_{\widetilde{\Xi A_i}}(\xi, \zeta) \geq \alpha\}$
    Optimize Eqs (22, 23) with objective function $E_n(\xi, \zeta)$ instead of u
    Corresponding α-cut of $\widetilde{B}_i$: $[\widetilde{B}_i]_\alpha = [B_{i,\alpha,1}, B_{i,\alpha,2}]$
  end for
  Assign fuzzy belief mass $\widetilde{m}_{E_n}(\widetilde{B}_i) = \widetilde{m}(\widetilde{\Xi A_i}) = m_\zeta(A_i)$
end for

3.4. Algorithm

The procedure to obtain the fuzzy mass function of the conditional expectation of output is summarized in two stages. Algorithm 1 constructs the gPC approximations $u_n(\xi, \zeta, y)$ and the corresponding $E_n(\xi, \zeta)$; Algorithm 2 then propagates the epistemic uncertainty through E_n to obtain the output fuzzy mass function $\widetilde{m}_{E_n}$.

4. Numerical examples

4.1. Example 1: epistemic UQ

Let us first look at the following example of a second order linear ordinary differential equation involving different epistemic uncertainties, where the uncertainty due to vagueness is represented using two fuzzy sets, and the uncertainty due to lack of knowledge is represented using one uncertain variable associated with a mass function.

$$u''(t) - 10u'(t) - \xi_1 u(t) = 4t$$

with initial conditions

$$u(0) = \zeta, u'(0) = \xi_2,$$

where ξ_1 is a fuzzy variable with the membership function μ_1

$$\mu_1(\xi_1) = \begin{cases} \frac{1}{5}\xi_1 - \frac{4}{5}, & \text{if } 4 \leq \xi_1 \leq 9, \\ -\frac{1}{5}\xi_1 + \frac{14}{5}, & \text{if } 9 \leq \xi_1 \leq 14, \\ 0, & \text{otherwise,} \end{cases}$$

and ξ_2 is another fuzzy variable with membership function μ_2

$$\mu_2(\xi_2) = \begin{cases} \frac{1}{2}\xi_2, & \text{if } 0 \leq \xi_2 \leq 2, \\ -\xi_2 + 3, & \text{if } 2 \leq \xi_2 \leq 3, \\ 0, & \text{otherwise.} \end{cases}$$

While ζ is a non-probabilistic uncertain variable associated with a mass function as

$$m_\zeta(A_1) = 0.2;\ m_\zeta(A_2) = 0.7;\ m_\zeta(A_3) = 0.1,$$

and its focal elements A_is are consecutive intervals

$$A_1 = [0.5, 0.8];\ A_2 = [0.8, 1.1];\ A_3 = [1.1, 1.4].$$

The goal is to quantify the uncertainty in the output solution u propagated from different types of epistemic uncertainty in inputs using the presented numerical method. Here, the analytical solution of the ODE is used directly as the forward model. We consider the solution value $u(t)$ at the fixed time t = 0.25 as the quantity of interest.

Under the assumption that the uncertain variables are independent, the two-dimensional fuzzy set is defined for $\xi = \{\xi_1, \xi_2\}$. Its support will be the tensor product of the supports for ξ_1 and ξ_2. The membership function is obtained by (illustrated in Figure 1(a)).

$$\mu(\xi_1, \xi_2) = \min(\mu_1(\xi_1), \mu_2(\xi_2)). \tag{32}$$

To quantify the epistemic uncertainty due to lack of knowledge, one can construct a mass function for u (i.e., find the output focal elements and assign the belief mass). However, due to the existence of other epistemic uncertainty caused by vagueness, the output focal elements are not crisp classical sets, but fuzzy sets. Specifically, a 3D fuzzy set is considered as an input focal element, where the classical set A_i is treated as a fuzzy set with a constant membership function one over the support. Then, Zadeh's extension principle can be applied to obtain one output fuzzy set, which will serve as one output fuzzy focal element with the same belief mass $m(A_i)$. In the numerical calculation, eleven α-cut levels are used to construct each output fuzzy focal element. For each α-cut, the corresponding output interval is obtained by solving a pair of optimization problems in Eqs (22) and (23). The optimization problems are solved using a sampling-based approach with a tensor grid of $30 \times 30 \times 50$ equally spaced points.

Figure 1(b) provides the obtained fuzzy mass function, which shows that u will fall in the fuzzy set $\widetilde{B}_2$ (corresponding to the input focal element $A_2 = [0.8, 1.1]$) with the maximum degree of belief 0.7 (red curve in Figure 1(b)), with preference going to its crisp subinterval $[3.91, 4.46]$ with a degree of membership one. The output u may also fall inside the other two focal elements (the fuzzy sets with membership functions in blue and orange curves in Figure 1(b)) with degrees of belief 0.2 and 0.1, respectively. Figure 1(c) shows the corresponding CBF and CPF (calculated with the Eqs (6), (7), (10) and (11)), which provide the lower and upper bounds of the possible true probability of the proposition that output u is below a fixed value.

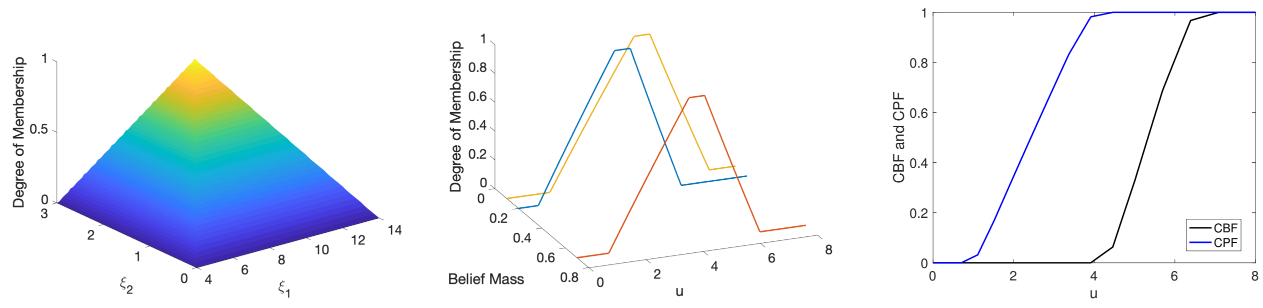

(a) **(b)** **(c)**

Figure 1. (a) The membership function for input 2D fuzzy variable $\xi = \{\xi_1, \xi_2\}$; (b) the fuzzy mass function for output u, where the three fuzzy focal elements with belief masses 0.7, 0.2, 0.1 are shown in red, blue and orange, respectively; and (c) the CBF and CPF for u.

4.2. Example 2: mixed aleatory and epistemic UQ

Now, we consider another second order ODE, which involves aleatory and various epistemic uncertainties.

$$\frac{d^2u(t,y,\zeta,\xi)}{dt^2} = yu,$$
$$u(0) = \zeta, u'(0) = \xi.$$

It is assumed that y is a random variable uniformly distributed over interval $[2, 5]$, and ξ is a fuzzy variable with the membership function μ given by

$$\mu(\xi) = \begin{cases} \xi - 1 & \text{if } 1 \le \xi \le 2, \\ -\frac{1}{3}\xi + \frac{5}{3} & \text{if } 2 \le \xi \le 5, \\ 0 & \text{otherwise,} \end{cases}$$

and ζ is another non-probabilistic uncertain variable associated with a mass function as

$$m_\zeta([0.4, 0.8]) = 0.2, m_\zeta([0.75, 1.15]) = 0.5, m_\zeta([1.1, 1.5]) = 0.3.$$

The mixed types of uncertainty in the output u at $t = 2$ are quantified using the proposed method. Specifically, a generalized polynomial chaos expansion is constructed to obtain $E_4(u|\xi, \zeta)$, which serves as an approximation of the true expectation $E(u|\xi, \zeta)$. Since the random variable is uniformly distributed, Legendre polynomials are chosen as the gPC basis. The gPC coefficients are estimated using a projection method, and the required integrals are approximated using Clenshaw-Curtis quadrature with seventeen Chebyshev points. With the obtained $E_4(u|\xi, \zeta)$, the output fuzzy sets are then constructed through α-cut optimization. Specifically, eleven α-cut levels are used to construct each output fuzzy set, and a tensor grid of 30×30 equally spaced points is used for the sampling-based optimization over each input α-cut. The resulting fuzzy mass function represents the epistemic uncertainty in the output expectation conditioned on the non-probabilistic uncertain variables ξ, ζ. For error analysis, the obtained fuzzy mass function is compared to a reference solution. The reference solution is computed using the available analytical solution of the ODE and the analytical expression for the conditional expectation. For the reference calculation, the optimization over each α-cut is performed using a finer tensor grid of 100×100 equally spaced points.

Figure 2(a) visualizes the output fuzzy mass function (shown by dashed curves) obtained using the proposed method, together with the reference fuzzy mass function (shown by solid curves). The close overlap between the two sets of curves indicates that the proposed method produces reliable results for this example. From the figure, one can observe that the conditional expectation will fall in three fuzzy focal elements with different degrees of belief. The fuzzy focal element with membership function plotted as the red curve has the highest degree of belief 0.5. Inside the fuzzy set, preference will be given to the crisp interval $[40.6, 49.7]$ with membership one. The corresponding CBF and CPF for $E_4(u|\xi, \zeta)$ are plotted as dashed curves in Figure 2(b). These curves also closely match the reference CBF and CPF, shown by solid curves. The CBF and CPF bound the possible true cumulative distribution function (CDF).

To illustrate the error bound of the approximated output fuzzy mass function established in Theorem 3.1, we compute the error in $\widetilde{m}_{E_n}$ for the conditional expectation of output u using Eq (17), together with the maximum L_2 norm error of the gPC expansion u_n over the support of each input fuzzy focal elements. All integrals involved in this calculation are evaluated using the Clenshaw-Curtis quadrature. The two errors are plotted with respect to the polynomial order n in Figure 2(c). One can observe that the gPC approximation u_n converges to the true solution u exponentially as expected, and the gPC error bounds the error in the output fuzzy mass function at every polynomial order, as predicted in Theorem 3.1.

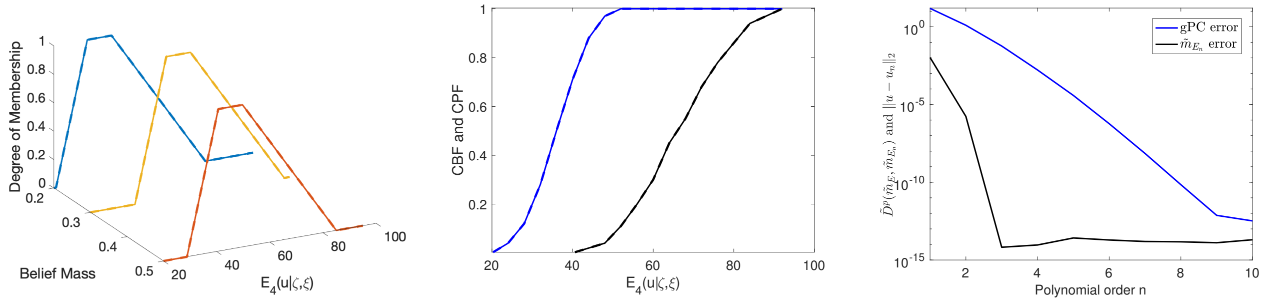

(a) **(b)** **(c)**

Figure 2. (a) The fuzzy mass function for $E_4(u|\xi,\zeta)$, where the three fuzzy focal elements with belief masses 0.5, 0.3, and 0.2 are shown in red, orange, and blue, respectively; (b) the CBF and CPF for $E_4(u|\xi,\zeta)$; and (c) the errors of output fuzzy mass function $\widetilde{D}_p(\widetilde{m}_E,\widetilde{m}_{E_n})$ and of gPC surrogate u_n with respect to n. In (a) & (b), the dashed curves are obtained from gPC approximation while the solid curves are from the reference solution.

5. Application to biological models

5.1. The Mitchell-Schaeffer model

In this section, we apply the proposed method to the Mitchell-Schaeffer model. Models of the cardiac membrane potential vary widely with respect to both mathematical complexity and level of physiological detail. Nearly all single-cell models are formulated as systems of ordinary differential equations (ODEs), drawing upon the famous Hodgkin-Huxley model of the nerve action potential. The Mitchell-Schaeffer equations [48] constitute a simple (two ODEs with five parameters) but surprisingly flexible model of the cardiac action potential. In particular, the Mitchell-Schaeffer model affords one the flexibility to (i) adjust the durations of the four phases of the action potential; (ii) simulate a variety of heart rhythms including normal 1:1 rhythm, alternans, or 2:1 conduction block; and (iii) fit data showing restitution of action potential duration (APD, explained below).

5.1.1. Basic equations

The Mitchell-Schaeffer model equations are

$$\frac{dv}{dt} = \frac{h}{\tau_{\text{in}}} v^2(1-v) - \frac{v}{\tau_{\text{out}}} + I_{\text{stim}}(t), \tag{33}$$

$$\frac{dh}{dt} = \begin{cases} (1-h)/\tau_{\text{open}} & \text{if } v \le v_{\text{gate}}, \\ -h/\tau_{\text{close}} & \text{if } v > v_{\text{gate}}. \end{cases} \tag{34}$$

Variable v represents transmembrane* potential, scaled such that 0 corresponds to the resting potential and 1 is the peak potential. The three terms on the right hand side represent currents: inward, outward, and stimulus, respectively. The inward current aggregates all transmembrane ionic currents, pumps, and exchangers that increase v (such as the fast sodium current and the L-type calcium current), and the outward current aggregates all currents that decrease v (such as the potassium current). The inward current is gated and regulated by the inactivation gate variable h, which varies between 0 and 1 according to Eq (34). The gate variable h increases toward 1 (i.e., the gates open) whenever v is below the threshold potential v_{gate}, and decays exponentially toward 0 whenever $v > v_{\text{gate}}$. The term $-v/\tau_{\text{out}}$, representing an outward current, is passive and ungated. The term I_{stim} represents a stimulus current, and here we presume that stimuli are applied impulsively, and periodically with period B. Both the strength and period are chosen such that every stimulus elicits an action potential. The four time constants are associated with the four phases of the action potential: τ_{in} for the rapid upstroke following a stimulus, τ_{close} for the plateau phase during which the inactivation gate h decays exponentially, τ_{out} for the semi-rapid repolarization during which the outward current dominates the inward current causing v to decrease, and τ_{open} for the reopening of the gates while $v \le v_{\text{gate}}$ prior to the next stimulus.

Figure 3(a) illustrates consecutive, simulated action potentials using Eqs (33) and (34), time constants $\tau_{\text{in}} = 0.1$ ms, $\tau_{\text{out}} = 2.4$ ms, $\tau_{\text{open}} = 100$ ms, $\tau_{\text{close}} = 150$ ms, and voltage threshold $v_{\text{gate}} = 0.13$. We define the *action potential duration (APD)* to be the amount of time during which $v \ge v_{\text{gate}}$ following a stimulus, and the *diastolic interval (DI)* to be the amount of time during which $v \le v_{\text{gate}}$ between consecutive action potentials. In a paced (i.e., repeatedly stimulated) cell, we let A_n denote the APD following the nth stimulus, and D_n the DI between the nth and $(n+1)$st action potentials; see the labels in Figure 3(a). Cardiac cells exhibit *restitution of APD* in that A_{n+1} depends upon D_n. Figure 3(b) illustrates this dependence via the *restitution curve*. The restitution curve can be obtained numerically by (i) solving Eqs (33) and (34) with a fixed pacing period until an approximate steady-state response is achieved; (ii) plotting the resulting pairs (D_n, A_{n+1}) for large n; and (iii) repeating the two preceding steps for various choices of the pacing period B. Figure 3(b) shows the numerically-obtained restitution curve obtained by letting B vary from 280 ms to 700 ms, and includes a second (barely distinguishable) curve obtained using asymptotic formulas (35) explained below.

The simplicity of the Mitchell-Schaeffer model makes it easy to estimate model parameters from restitution data. The process is facilitated by asymptotic formulas for the restitution curve that are incredibly accurate under the physiologically reasonable assumption that $\tau_{\text{in}} \ll \tau_{\text{out}} \ll \tau_{\text{close}}$. Let $\epsilon = \tau_{\text{out}}/\tau_{\text{close}}$ and $h_{\min} = 4\tau_{\text{in}}/\tau_{\text{out}}$, and define $h(DI_n) = 1 - (1 - h_{\min})\exp(-DI_n/\tau_{\text{open}})$. Then, as shown in [49], in the limit $\epsilon \to 0$, we have the [non-regular] perturbation expansion $APD_{n+1} \sim f_0(DI_n) + \varepsilon^{2/3} f_1(DI_n)$, where

$$f_0(DI) = \tau_{\text{close}} \ln\left[\frac{h(DI)}{h_{\min}}\right], \qquad f_1(DI) = \zeta\tau_{\text{close}}\left[\frac{1 - e^{-DI/\tau_{\text{open}}}}{h(DI)}\right], \tag{35}$$

and $\zeta = 2.33811...$ is a root of the Airy function $Ai(-x)$.

*The usual convention is to define this voltage as intracellular potential minus extracellular potential.

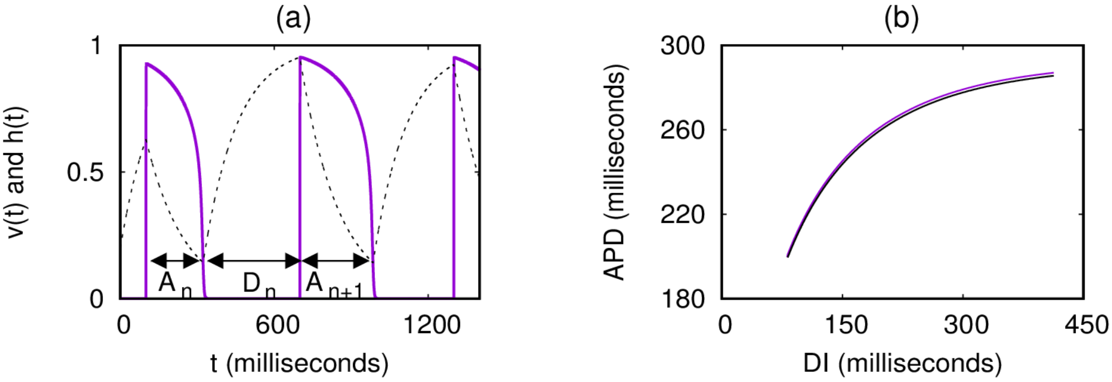

Figure 3. (a) Consecutive action potentials generated by numerical simulation of the Mitchell-Schaeffer model equations (33) and (34). Voltage versus time (purple, solid, thick curve) and the gate variable (black, dashed, thin curve) are shown. APD following the nth stimulus is indicated by A_n, and the subsequent DI is indicated by D_n. (b) Restitution curve using the same parameters as in the other panel, but for various choices of $B \in [280, 700]$. Two barely distinguishable curves are shown: one obtained by numerical solution of the model equations, and one from the asymptotic formula (35).

5.1.2. Parameter ranges and distributions

For the purpose of performing uncertainty quantification for the Mitchell-Schaeffer model, we use fuzzy sets and mass functions to represent different types of epistemic uncertainty in the model, and probability density functions to represent stochastic uncertainty. The uncertainties are propagated through the model and accumulated in the quantity of interest: steady-state APD after long-term pacing with period $B = 600$ ms. We presume that $v_{\text{gate}} = 0.13$ and sample the values of the time constants τ_{in}, τ_{close}, τ_{out}, and τ_{open} from four distributions. For every parameter set that we consider, constant pacing with period $B = 600$ ms yields a steady-state in which every stimulus elicits an action potential, and APD remains constant. Additionally, the ranges and distributions of the four parameters are meant to ensure that steady-state APD is physiologically reasonable for typical mammals (e.g., 200 ms for rabbit ventricular myocytes). To this end, the relation $APD + DI = B$ coupled with the asymptotic approximation $APD_{n+1} \sim f_0(DI_n) + \varepsilon^{2/3} f_1(DI_n)$ given by (35) informs parameter selection. We use the following ranges and distributions for the four time constant parameters, all of which are measured in milliseconds:

- $\tau_{\text{in}} \in \widetilde{A}$, where the membership function for the fuzzy set (see Figure 4(a)) is

$$\mu(\tau_{\text{in}}) = 0.15/\tau_{\text{in}} - 0.5, \qquad \tau_{\text{in}} \in [0.1, 0.3]. \tag{36}$$

- τ_{open} is associated with a mass function (see Figure 4(b)), which has three focal elements:

$$B_1 = [100, 133], \qquad B_2 = [133, 167], \qquad B_3 = [167, 200]. \tag{37}$$

Their corresponding belief masses are

$$m_{\tau_{\text{open}}}(B_1) = 0.5, \qquad m_{\tau_{\text{open}}}(B_2) = 0.3, \qquad m_{\tau_{\text{open}}}(B_3) = 0.2. \tag{38}$$

- τ_{out} is a random variable with a Gaussian distribution $\tau_{\text{out}} \sim \mathcal{N}(3.5, 0.33)$.
- τ_{close} is also random associated with a Gaussian distribution $\tau_{\text{close}} \sim \mathcal{N}(150, 12.0)$. The joint Gaussian distribution for the random variables is visualized in Figure 4(c).

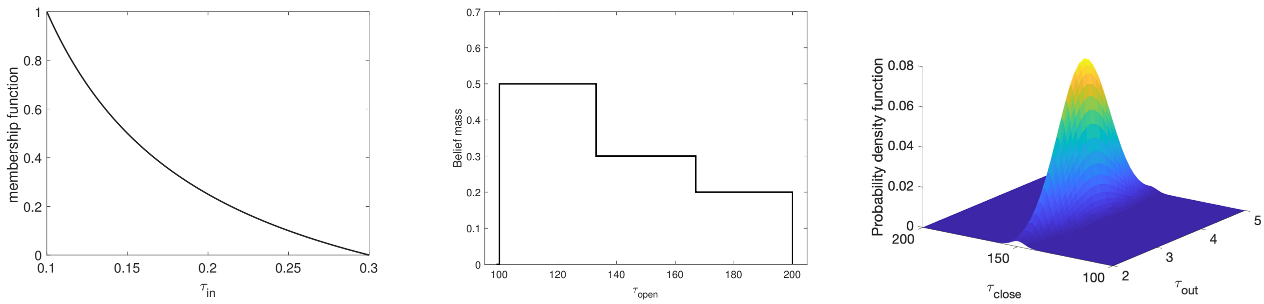

(a) **(b)** **(c)**

Figure 4. (a) Membership function for τ_{in}; (b) the mass function for τ_{open}; and (c) probability density function for $\{\tau_{\text{close}}, \tau_{\text{out}}\}$.

The distributions of the uncertain parameters in the Mitchell-Schaeffer model are selected based on prior studies in the literature [50–52] and chosen to ensure that the resulting steady-state APD is physiologically reasonable for typical mammals. For example, in spatially extended tissue, the parameter τ_{in} has a strong influence on the propagation speed of action potentials [53]. The membership function for τ_{in} is therefore biased toward values that elicit reasonable propagation speeds for mammalian ventricular tissue, since propagation speed would become unrealistically low if τ_{in} exceeds 0.3. The selected membership function also produces reasonable APD values under the pacing protocol considered in this study. The parameter τ_{open} has little effect on APD, but does affect the slope of the restitution curve, a quantity known to influence the likelihood of abnormal rhythms such as T-wave alternans. The belief function for τ_{open} is chosen to avoid slopes that would be regarded as extreme for most mammals, while acknowledging that estimates of τ_{open} can vary by a factor of two across datasets [52]. In addition, prior experimental studies [51] suggest that variability of baseline APD across human subjects may be approximated using a normal distribution, and the leading-order asymptotics (see the function f_0 defined in (35)) suggest that APD should scale roughly proportionally to τ_{close}. Guided by this information, the uncertainty representations for the parameters are assumed to serve as part of the input to the proposed UQ framework. For the above ranges and distributions of parameters, we have $0.08 \leq h_{\min} \leq 0.6$. In our simulations, steady-state APD values as low as 120 ms or as high as 400 ms would be considered extreme, and "typical" steady-state values are physiologically reasonable.

5.1.3. Mixed uncertainty quantification in APD

With the proposed method, we quantify the mixed uncertainty in APD propagated from both aleatory and epistemic uncertainty in the uncertain input parameters. To reduce the computational cost, we construct gPC expansion using Hermite polynomials with order $n = 4$ to serve as the approximation to APD in the stochastic space and correspondingly, the conditional expectation $E_4(APD|\tau_{\text{in}}, \tau_{\text{open}})$. The gPC coefficients are estimated using a least-squares approach with 100 data points. As an example, we show the surface of the constructed APD approximation with respect to two random parameters, τ_{out} and τ_{close}, at a fixed value for the non-probabilistic parameters $\tau_{\text{in}} = 0.1$ and $\tau_{\text{open}} = 100$ in Figure 5(a). The corresponding cumulative distribution function (CDF) using the constructed gPC expansion evaluated at 200,000 random samples is obtained and plotted in Figure 5(b). With the constructed gPC expansions, the expectation of APD in stochastic space at any fixed $\tau_{\text{in}}, \tau_{\text{open}}$ can also be estimated without extra effort. For the purpose of illustration, the conditional expectation of APD (the surface) is plotted in Figure 5(c) with respect to non-probabilistic uncertain parameters, respectively. It shows that the uncertainty in τ_{in} has relatively more impact on the variation in the conditional expectation of APD compared to τ_{open}.

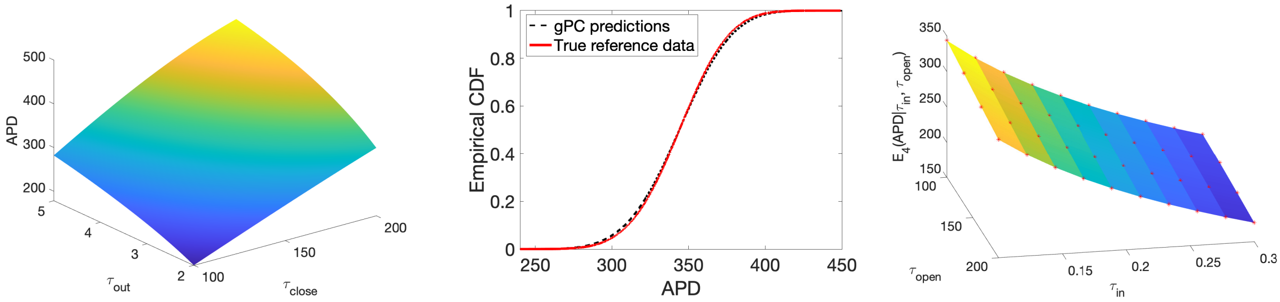

(a) **(b)** **(c)**

Figure 5. (a) The gPC surface of APD over the stochastic space at fixed $\tau_{\text{in}} = 0.1$ and $\tau_{\text{open}} = 100$; (b) the CDF obtained from the gPC expansion (black-dashed curve) and from the reference solution (red-solid curve), each evaluated at 200,000 random samples from stochastic space at the same fixed values of τ_{in} and τ_{open}; and (c) surface of the conditional expectation of APD as a function of τ_{in} and τ_{open} predicted by the gPC expansion; red asterisks mark the reference expectations from Monte Carlo sampling method with 200,000 samples.

To quantitatively validate the accuracy of gPC approximation, we generate 200,000 random samples from stochastic space of $\{\tau_{\text{out}}, \tau_{\text{close}}\}$ at forty fixed representative combinations of epistemic variables, and obtain the corresponding output APD as reference datasets. The relative L_2-norm errors of the surrogate predictions at four representative values for $\tau_{\text{in}}, \tau_{\text{open}}$ are reported in Table 2. All relative errors for forty combinations are below 0.6%, so the constructed gPC surrogate model is considered sufficiently accurate for the uncertainty analysis.

Table 2. Error induced by gPC surrogate for APD.

	$\tau_{\text{in}} = 0.1$ $\tau_{\text{open}} = 100$	$\tau_{\text{in}} = 0.17$ $\tau_{\text{open}} = 133$	$\tau_{\text{in}} = 0.23$ $\tau_{\text{open}} = 167$	$\tau_{\text{in}} = 0.30$ $\tau_{\text{open}} = 200$
gPC error	0.56%	0.57%	0.57%	0.56%
Expectation error	0.030%	0.027%	0.029%	0.034%

As an illustrative example, Figure 5(b) compares the empirical CDF of the gPC output predicted at those 200,000 random samples with fixed $\tau_{\text{in}} = 0.1, \tau_{\text{open}} = 100$ to that of the corresponding reference data set for the fixed $\tau_{\text{in}} = 0.1, \tau_{\text{open}} = 100$. The predicted CDF nearly overlaps with the reference CDF, indicating good agreement between the surrogate and the full model evaluations. In addition, the corresponding relative error in the estimated expectation compared with the Monte Carlo estimate is also reported and is bounded by 0.1%. The expectation values at forty combinations of epistemic variables computed from Monte Carlo sampling are marked as red asterisks in Figure 5(c), providing a visual validation of the expectation surface obtained from the gPC surrogate.

Utilizing the constructed numerical approximation for the conditional expectation, we can obtain the output expectation fuzzy mass function efficiently. Specifically, ten α-cut levels are used to construct each output fuzzy set, and sampling-based method with a tensor grid of 10×10 equally spaced points are implemented to obtain the lower and upper bounds of output fuzzy set α-cuts. The fuzzy mass function for $E(APD|\tau_{\text{in}}, \tau_{\text{open}})$ is plotted in Figure 6(a). One can observe that the conditional expectation of APD falls inside the fuzzy set $\widetilde{B}_1$ with a membership function shown as the blue curve with belief mass 0.5, which corresponds to $\tau_{\text{open}} \in B_1$. The preference is given to $[334.6, 343.5]$ with a degree of membership one. It may also be inside the fuzzy set $\widetilde{B}_2$ (see the red curve in Figure 6(a)) with belief mass 0.3, with further preference on $[325.4, 334.6]$. In addition, the conditional expectation of APD may also be in the fuzzy set $\widetilde{B}_3$ (see orange curve in Figure 6(a)) with belief mass 0.2. The preference inside this fuzzy set is the interval $[317, 325.4]$. The corresponding CBF and CPF are visualized in Figure 6(b), which bound the possible true cumulative distribution function that measures the probability of $E(APD|\tau_{\text{in}}, \tau_{\text{open}})$ being below a fixed value.

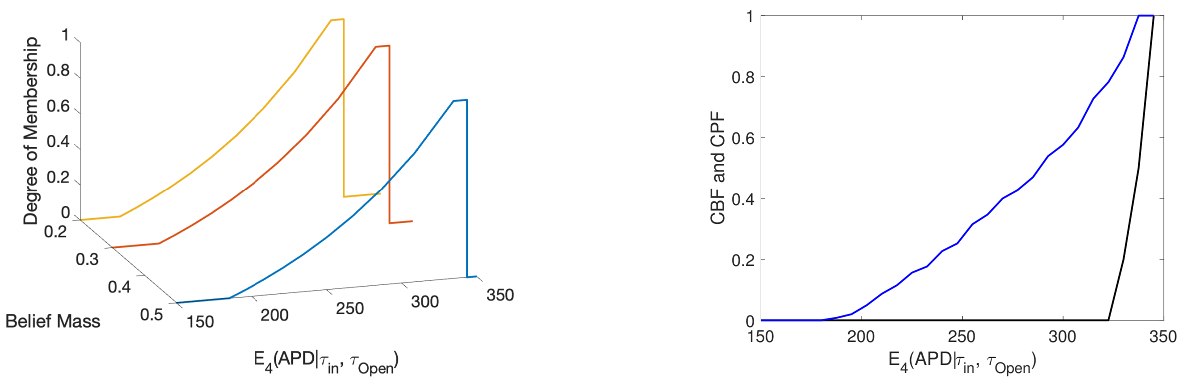

(a) **(b)**

Figure 6. (a) The fuzzy mass function for $E(APD|\tau_{\text{in}}, \tau_{\text{open}})$, where the three fuzzy focal elements with belief masses 0.5, 0.3, and 0.2 are shown in blue, red, and orange, respectively; and (b) the CBF (black curve) and CPF (blue curve).

APD measures the duration for which the cardiac membrane potential remains above the threshold value after stimulation, and could be influenced by uncertain time constants that control different phases of action potential. As shown in Figure 6(a), the uncertainty in the gate-reopening constant τ_{open} induces a mild shift between the output fuzzy focal elements. The spread within each output fuzzy focal element for the steady-state APD is primarily corresponding to the fuzzy uncertainty in τ_{in}, which is associated with the rapid upstroke dynamics. The moderate differences among the fuzzy focal elements compared with the relatively larger spread within each fuzzy focal element, together with the comparison between the variation in APD along τ_{in} and τ_{open} directions in Figure 5(c), indicate that the dynamics associated with the rapid upstroke parameter τ_{in} has a more substantial effect on APD. This makes sense on biophysical grounds, in that the parameters τ_{in} and τ_{out} regulate the depolarizing and repolarizing currents (respectively) that fluctuate during an action potential, while τ_{open} is associated with behavior that occurs during the diastolic interval, **not** during the action potential. The resulting fuzzy mass function and the CBF/CPF curves provide ranges of possible APD values, along with the associated membership values and degrees of belief. These results can be used to assess whether the predicted APD remains within a physiologically reasonable range under uncertainty, and to quantify the lower and upper bounds of probability that APD values fall outside that range.

5.2. A computational model of olfaction

Marine crustaceans and insects use arrays of chemosensory hairs to extract chemical cues (odors) from the surrounding environment. This process is influenced by various factors such as hair morphology and surrounding fluid characteristics. Understanding how uncertainty in these parameters propagates through the system to uncertainties in the fluid flow and odor transport is critical for robust model-based inference and for advancing biological insight.

5.2.1. Basic equations

The fluid regime of odor capture by hair arrays is governed by the following incompressible Navier-Stokes equations

$$\rho\left(u_t(x,t) + u(x,t)\cdot\nabla u(x,t)\right) = -\nabla p(x,t) + \hat{\mu}\nabla^2 u(x,t) + F(x,t), \tag{39}$$

$$\nabla\cdot u(x,t) = 0, \tag{40}$$

where $p(x,t)$ denotes pressure, $u(x,t)$ is the fluid velocity, ρ denotes the fluid density, $\hat{\mu}$ is the dynamic viscosity, and $F(x,t)$ denotes the external force defined by

$$F(x,t) = \int f(s,t)\delta(x - X(s,t))ds, \tag{41}$$

$$X_t(s,t) = u(X(s,t)) = \int u(x,t)\delta(x - X(s,t))dx, \tag{42}$$

with $X(s,t)$ the Cartesian coordinates at time t of the boundary point labeled by the Lagrangian parameter s, and $f(s,t)$ the force per unit length applied to the boundary of the fluid. Forces are spread from the boundary and the fluid grid via a two-dimensional Dirac delta function δ.

The three-dimensional hair structure consists of long sensilla (sensory hairs) protruding from a central, supporting antenna. For simplicity, we analyze a cross-sectional slice through the antenna and sensilla, yielding a two-dimensional representation with circular cross-sections of the antenna (large circle) and sensilla (small circles) (see Figure 7 for a three-hair-array model as an example). Dirichlet boundary conditions at the x-axis boundaries are imposed to produce horizontal, free-stream flow passing the sensilla array. Velocity at these boundaries is quickly accelerated from 0 to the final, steady-state flow of 0.06 ms^{-1}, a speed representative of sampling in this regime [54, 55]. Simulations are implemented using Immersed Boundary with Adaptive Mesh Refinement (IBAMR) software, which is an open-source, C++ framework that enables advanced modeling of fluid-structure interactions using IBM [56, 57]. Each simulation is allowed to reach the steady state. In order to investigate the effects of size and flow speeds, Reynolds number is varied over the range reported in the literature. For more details on this model, see Waldrop et al. [58].

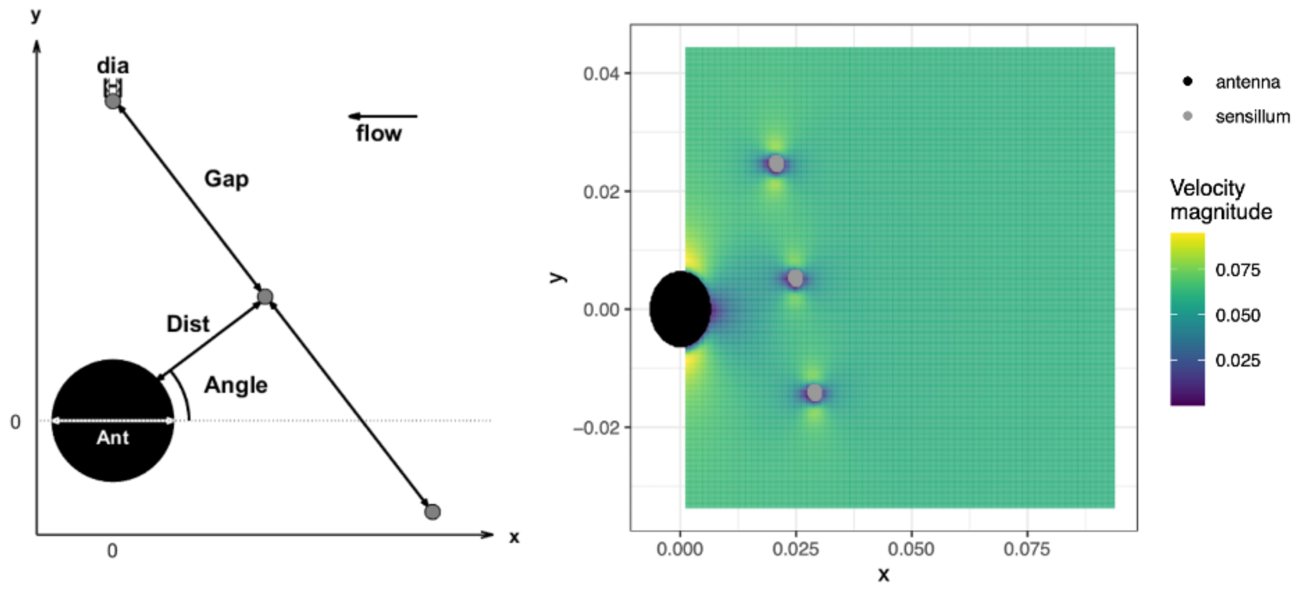

Figure 7. (a) Hair structure: supporting antenna (black) and three sensilla (gray), and several morphological parameters dia, Ant, Dist, Angle, and Gap; and (b) an example of simulated velocity field with Angle = 12.0316, Gap = 8.92807, Ant = 5.92511, Dist = 0.01861956, and Re = 1.386137.

5.2.2. Parameter ranges and distributions

The mixed uncertainty in the model is represented using the hair-array morphological parameters and flow characteristics. Specifically, fuzzy sets and mass functions are used to represent different types of epistemic uncertainty while probability density functions are used to model the stochastic uncertainty. For the morphological parameters (see Figure 7(a)), the array angle (Angle), defined as the orientation of the array relative to the oncoming flow, is treated as uncertain due to natural variability and measurement error. Its uncertainty is represented with a mass function (see Figure 8(a)), which has three focal elements:

$$B_1 = [0, 45], \qquad B_2 = [45, 90], \qquad B_3 = [90, 180]. \tag{43}$$

Their corresponding belief masses are

$$m_{\text{Angle}}(B_1) = 0.8, \qquad m_{\text{Angle}}(B_2) = 0.18, \qquad m_{\text{Angle}}(B_3) = 0.02. \tag{44}$$

We fix each sensillum's diameter and arrange the array with uniform spacing; we then nondimensionalize the spacing by the diameter and denote the gap-to-hair-diameter-ratio as Gap.

Based on experts' opinions, we assume Gap $\in \widetilde{A}$, where the membership function for the fuzzy set (see Figure 8(b)) is

$$\mu(\text{Gap}) = \begin{cases} 0.25\text{Gap} - 0.25, & 1 \leq \text{Gap} \leq 5, \\ 1, & 5 < \text{Gap} \leq 15, \\ -1/35\text{Gap} + 10/7, & 15 < \text{Gap} \leq 50. \end{cases}$$

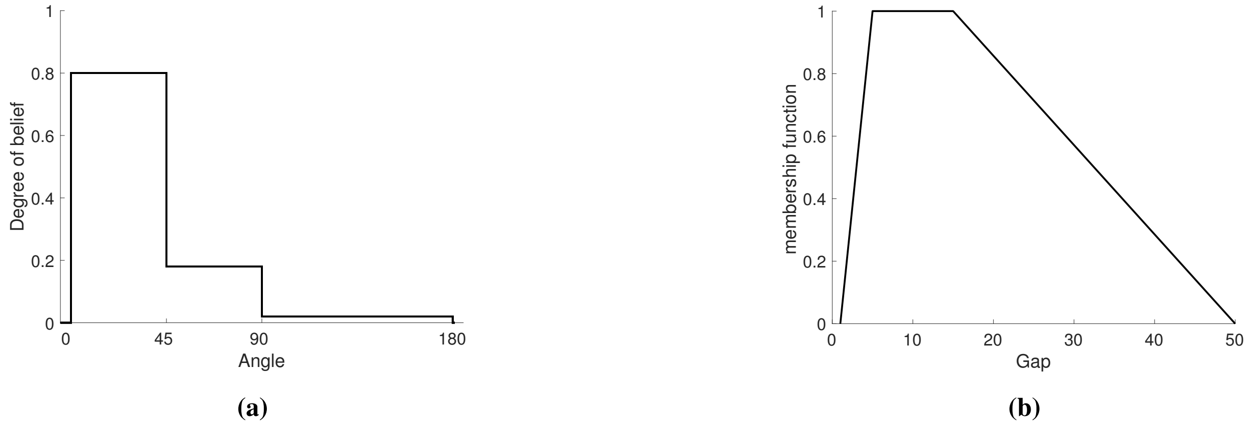

Figure 8. (a) The mass function for Angle; and (b) the membership function for Gap.

Additionally, we define Ant as the ratio of the antenna diameter to *dia*, and Dist as the ratio of the distance from the edge of the innermost sensillum to the antenna to *dia*. Due to the morphological variability in insects, Ant and Dist are treated as non-deterministic. Together with the Reynolds number *Re*, they are modeled as random variables and are assumed to follow a uniform distribution as follows:

$$\text{Ant} \sim \mathcal{U}([1, 50]), \qquad \text{Dist} \sim \mathcal{U}([0.001, 0.02]), \qquad Re \sim \mathcal{U}([0.1, 10]). \tag{45}$$

Note that the ranges of these parameters are taken from studies on various species in the literature, including crabs [55, 59–62], lobsters [54, 63–65], crayfish [66–69], among others [70–73]. Based on these values, available biological knowledge, and expert experience, the further distributions of the uncertain parameters inside the whole ranges are assumed. Rigorous distinction and construction of mathematical representations is out of the scope of this work. These assumptions serve as part of the input to the UQ framework. The UQ analysis for this application is based on the assumed distributions for the uncertain variables. Better-supported assumptions informed by additional biological data would lead to more biologically reasonable uncertainty analysis.

5.2.3. Mixed uncertainty quantification in leakiness

With the simulated fluid velocity fields (see Figure 7(b) as an example), quantities related to fluid flow through and around the hair array, such as leakiness, are computed with VisIt and R [74, 75]. Leakiness is defined as the ratio of the area of fluid that passes through the array during the simulation to the area of fluid that would have passed through the same area in the absence of the array. Numerically, velocities are evenly sampled along the line through the sensilla array using VisIt, then are multiplied by the simulation duration ($t = 0.025$) and the inter-sample spacing. Summing these contributions yields the area swept by the fluid in the simulation. Similarly, the unobstructed reference area is computed using the imposed free-stream speed (0.06 ms^{-1}).

With the proposed method, we quantify mixed uncertainty in leakiness propagated from both aleatory and epistemic uncertainty in the non-deterministic morphological parameters and Reynolds number. To reduce the computational cost, we construct a gPC expansion using Legendre polynomials with order $n = 5$ to serve as a surrogate for leakiness, where gPC coefficients are also estimated using a least-squares approach with 2000 points. With the absence of additional testing data for this application, to quantify the accuracy of gPC approximations, K-fold cross-validation is employed since it is one of "the simplest and most widely used methods for estimating prediction error [76]". We take $K = 10$ here, as recommended in [76]. Specifically, the full data set from 2000 CFD simulations is split into ten equal-sized subsets. For each subset, we use the remaining nine subsets to construct a gPC expansion and calculate the prediction error of the gPC on the chosen subset. The relative prediction error for each of the ten subsets is reported in Table 3. The constructed gPC expansion approximation for leakiness is also considered as reasonably accurate due to low relative error.

Table 3. Prediction error of gPC for leakiness from ten-fold cross validation.

Subset index	1	2	3	4	5	6	7	8	9	10
Error	4.5%	3.4%	3.7%	4.4%	3.7%	4.3%	4.0%	3.4%	4.0%	3.6%

With eleven α-cut levels, sampling-based optimizations with a tensor grid of 20×60 points are implemented to obtain the fuzzy mass function of the output expectation. The numerical approximation fuzzy mass function for E(Leakiness|Angle, Gap) is plotted in Figure 9(a), which indicates that the conditional expectation of leakiness falls in the fuzzy set (membership function shown as blue curve) with the highest degree of belief 0.8. Within the fuzzy set, the preference is given to [0.60, 0.93] with a degree of membership one. Figure 9(b) provides the corresponding CBF and CPF, which bounds the possible true CDF of E(Leakiness|Angle, Gap).

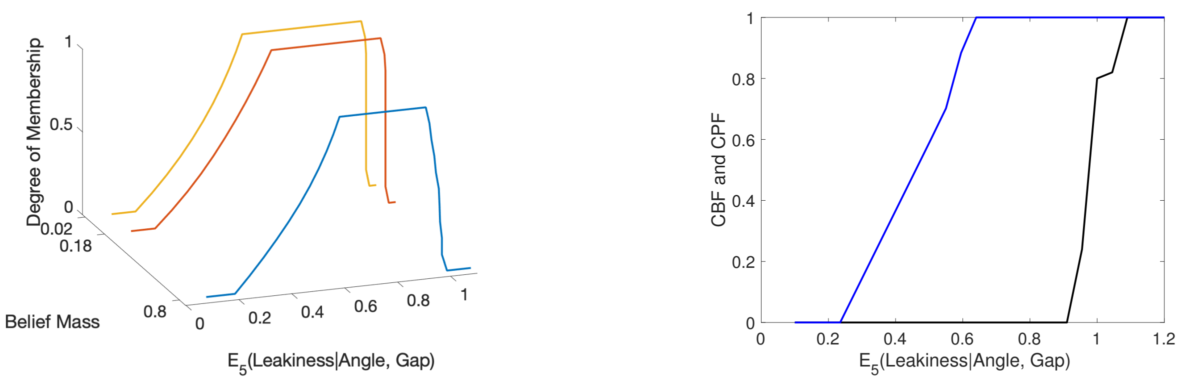

Figure 9. Uncertainty representation for E_5(Leakiness|Angle, Gap): (a) the fuzzy mass function, where the three fuzzy focal elements with belief masses 0.8, 0.18, and 0.02 are shown in blue, red, and orange, respectively; and (b) the corresponding CBF (black curve) and CPF (blue curve).

For many insects and marine crustaceans, chemosensory sensilla arrays sample odorant-laden flow from the surrounding environment. Leakiness measures the degree of fluid penetration through the array and serves as a proxy for the exposure of sensory hairs to the fluid flow. The morphological parameters of the array have potential influence on leakiness and consequently, the odor-sampling performance. In particular, uncertainty in Gap varies the spacing available for flow penetration, and uncertainty in Angle varies the orientation of the array relative to the incoming flow and may alter the exposure of sensilla to the fluid. Figure 9(a) suggests that the steady-state leakiness fuzzy focal elements associated with different Angle focal elements are relatively close to each other and overlap substantially, while the spread of leakiness within each fuzzy mass function, primarily influenced by the fuzzy variable Gap, is comparatively larger. This provides a qualitative indication that, under this uncertainty model, vagueness in Gap has a more visible effect on the leakiness than the uncertain variable Angle. This observation is consistent with physical intuition that hair spacing (Gap) strongly influences the permeability of flow through the array. The resulting fuzzy mass function characterizes the odor-sampling performance under uncertainty in morphological parameters and flow conditions. In particular, the range with membership value one and high belief mass indicates that the hair array is likely to remain moderately to highly permeable to the surrounding flow under the assumed uncertainty model.

This study is based on a two-dimensional cross-sectional model and may not capture all features of the full three-dimensional fluid flow through chemosensory hair arrays. The proposed UQ framework, however, is non-intrusive and is not restricted by the spatial dimensionality of the underlying forward problem. The same framework can be applied to a three-dimensional Navier-Stokes model by replacing each two-dimensional forward solver. The main additional cost would arise from the increased expenses of each forward model evaluation, while the number of evaluations is primarily influenced by the dimension of the uncertain input space. Extending this analysis to a full three-dimensional olfaction model is a possible direction of future work.

6. Summary and conclusions

The propagation of uncertainty can be challenging when randomness, vagueness, and incomplete knowledge coexist in the same computational model. Although probability theory, fuzzy set theory and Dempster-Shafer theory have each been used individually or in pairs successfully in uncertainty propagation, a unified computational treatment of these three different forms of uncertainty remains limited. In this work, we address this issue by developing an efficient framework to quantify stochastic uncertainty and two distinct epistemic uncertainties within a common setting using fuzzy mass functions for output expectation. In addition, error analysis is conducted to assess the quality of the numerical approximation. Several numerical examples are included to demonstrate the method, followed by applications to the Mitchell-Schaeffer ODE model and a PDE model of olfaction.

The proposed algorithm is implemented under the assumption that the uncertain variables are independent when combining and propagating the uncertainty. In biological systems, however, some biological parameters may exhibit dependence due to body proportions, developmental constraint, physiological mechanisms, or species-specific morphology. Ignoring such dependence may affect the propagated uncertainty associated with the output quantities. In our biological examples, the independence is assumed, and the assumption provides a reasonable approximation because the parameter ranges are carefully selected to represent biologically plausible configurations, and each of the two biological models is intended to cover a broad range of organisms rather than a single species-specific setup. When sufficient joint data corresponding to biological parameters become available, extending the proposed algorithm to incorporate dependence among uncertain variables will be an interesting direction for future work.

Although the proposed algorithm is theoretically applicable to high-dimensional problems, its computational cost may increase substantially with the dimension of both stochastic and non-stochastic uncertainty spaces. In particular, the gPC method may suffer from the curse of dimensionality as the stochastic dimension increases, while the number of focal elements and consequently, the number of optimization problems, may grow exponentially with the dimension of non-stochastic space. The sampling strategy used in the optimization process can further increase the computational burden as the number of optimization variables increases. These challenges may be addressed in future work through sparse-grid integration for gPC expansions, sensitivity-analysis based reduction of non-influential uncertain variables in the framework of DS theory, and more efficient optimization strategies.

Use of AI tools declaration

The authors declare they have not used Artificial Intelligence (AI) tools in the creation of this article.

Acknowledgments

Research was sponsored by the Army Research Office and was accomplished under Grant Number W911NF-22-1-0037. The views and conclusions contained in this document are those of the authors and should not be interpreted as representing the official policies, either expressed or implied, of the Army Research Office or the U.S. Government. The U.S. Government is authorized to reproduce and distribute reprints for Government purposes notwithstanding any copyright notation herein. This work was also supported by National Science Foundation (DMS-2152040 and DMS-2152110).

Conflict of interest

The authors declare there is no conflict of interest.

References

1. J. Jakeman, M. Eldred, D. Xiu, Numerical approach for quantification of epistemic uncertainty, *J. Comput. Phys.*, **229** (2010), 4648–4663. https://doi.org/10.1016/j.jcp.2010.03.003
2. M. S. Eldred, L. P. Swiler, G. Tang, Mixed aleatory-epistemic uncertainty quantification with stochastic expansions and optimization-based interval estimation, *Reliab. Eng. Syst. Saf.*, **96** (2011), 1092–1113. https://doi.org/10.1016/j.ress.2010.11.010
3. C. Wang, Z. Qiu, Y. He, Fuzzy interval perturbation method for the uncertain heat conduction problem with interval and fuzzy parameters, *Int. J. Numer. Methods Eng.*, **104** (2015), 330–346. https://doi.org/10.1002/nme.4932

4. C. Baudrit, D. Dubois, D. Guyonnet, Joint propagation and exploitation of probabilistic and possibilistic information in risk assessment, *IEEE Trans. Fuzzy Syst.*, **14** (2006), 593–608. https://doi.org/10.1109/TFUZZ.2006.876720
5. C. J. Roy, W. L. Oberkampf, A comprehensive framework for verification, validation, and uncertainty quantification in scientific computing, *Comput. Methods Appl. Mech. Eng.*, **200** (2011), 2131–2144. https://doi.org/10.1016/j.cma.2011.03.016
6. W. L. Oberkampf, J. C. Helton, K. Sentz, Mathematical representation of uncertainty, in *Proceedings of the AIAA Non-Deterministic Approaches Forum AIAA 2001-1645*, AIAA, (2001), 1645. https://doi.org/10.2514/6.2001-1645
7. L. A. Zadeh, Fuzzy sets, *Inf. Control*, **8** (1965), 338–353. https://doi.org/10.1016/S0019-9958(65)90241-X
8. P. Walley, G. de Cooman, A behavioural model for linguistic uncertainty, *Inf. Sci.*, **134** (2001), 1–37. https://doi.org/10.1016/S0020-0255(01)00090-1
9. G. Shafer, *A Mathematical Theory of Evidence*, Princeton University Press, NJ, USA, 1976. https://doi.org/10.1515/9780691214696
10. A. P. Dempster, Upper and lower probabilities induced by a multivalued mapping, *Ann. Math. Stat.*, **38** (1967), 325–339. https://doi.org/10.1214/aoms/1177698950
11. X. Su, S. Shang, L. Xiong, Z. Hong, J. Zhong, Research on dependent evidence combination based on principal component analysis, *Math. Biosci. Eng.*, **21** (2024), 4853–4873. https://doi.org/10.3934/mbe.2024214
12. D. Dubois, H. Prade, *Possibility Theory: An Approach to Computerized Processing of Uncertainty*, Plenum Press, New York, 1988.
13. D. Dubois, Possibility theory and statistical reasoning, *Comput. Stat. Data Anal.*, **51** (2006), 47–69. https://doi.org/10.1016/j.csda.2006.04.015
14. S. Destercke, D. Dubois, E. Chojnacki, Unifying practical uncertainty representations: I. generalized p-boxes, *Int. J. Approx. Reason.*, **49** (2008), 649–663. https://doi.org/10.1016/j.ijar.2008.07.003
15. N. Wiener, The homogeneous chaos, *Am. J. Math.*, **60** (1938), 897–936. https://doi.org/10.2307/2371268
16. D. Xiu, G. Karniadakis, The Wiener-Askey polynomial chaos for stochastic differential equations, *SIAM J. Sci. Comput.*, **24** (2002), 619–644. https://doi.org/10.1137/S1064827501387826
17. L. Mathelin, M. Y. Hussaini, A stochastic collocation algorithm for uncertainty analysis, in *Technical Report NASA/CR-2003-212153*, NASA Langley Research Center, 2003.
18. R. Schöbi, B. Sudret, J. Wiart, Polynomial-chaos-based kriging, *Int. J. Uncertain. Quantif.*, **5** (2015), 171–193. https://doi.org/10.1615/Int.J.UncertaintyQuantification.2015012467
19. K. Weise, E. Müller, L. Poßner, T. R. Knösche, Comparison of the performance and reliability between improved sampling strategies for polynomial chaos expansion, *Math. Biosci. Eng.*, **19** (2022), 7425–7480. https://doi.org/10.3934/mbe.2022351

20. Y. He, M. Y. Hussaini, Mixed aleatory and epistemic uncertainty propagation using Dempster–Shafer theory, *J. Comput. Appl. Math.*, **429** (2023), 115234. https://doi.org/10.1016/j.cam.2023.115234
21. A. Talavera, R. Aguasca, B. Galván, A. Cacereño, Application of Dempster-Shafer theory for the quantification and propagation of the uncertainty caused by the use of AIS data, *Reliab. Eng. Syst. Saf.*, **111** (2013), 95–105. https://doi.org/10.1016/j.ress.2012.10.007
22. J. Tang, Z. Wu, C. Yang, Epistemic uncertainty quantification in flutter analysis using evidence theory, *Chin. J. Aeronaut.*, **28** (2015), 164–171. https://doi.org/10.1016/j.cja.2014.12.024
23. N. B. Abdallah, N. Mouhous-Voyneau, T. Denoeux, Using Dempster-Shafer theory to model uncertainty in climate change and environmental impact assessments, in *Proceedings of the 16th International Conference on Information Fusion*, IEEE, (2013), 2117–2124.
24. H. R. Bae, R. V. Grandhi, R. A. Canfield, Uncertainty quantification of structural response using evidence theory, *AIAA J.*, **41** (2003), 2062–2068. https://doi.org/10.2514/2.1898
25. S. Adhikari, H. H. Khodaparast, A spectral approach for fuzzy uncertainty propagation in finite element analysis, *Fuzzy Sets Syst.*, **243** (2014), 1–24. https://doi.org/10.1016/j.fss.2013.10.005
26. S. Dey, T. Mukhopadhyay, H. H. Khodaparast, S. Adhikari, Fuzzy uncertainty propagation in composites using Gram-Schmidt polynomial chaos expansion, *Appl. Math. Model.*, **40** (2016), 4412–4428. https://doi.org/10.1016/j.apm.2015.11.038
27. Y. He, M. Mirzargar, R. M. Kirby, Mixed aleatory and epistemic uncertainty quantification using fuzzy set theory, *Int. J. Approx. Reason.*, **66** (2015), 1–15. https://doi.org/10.1016/j.ijar.2015.07.002
28. R. R. Shrestha, A. Bárdossy, F. Nestmann, Analysis and propagation of uncertainties due to the stage–discharge relationship: A fuzzy set approach, *Hydrol. Sci. J.*, **52** (2007), 595–610. https://doi.org/10.1623/hysj.52.4.595
29. C. Wang, H. G. Matthies, Epistemic uncertainty-based reliability analysis for engineering system with hybrid evidence and fuzzy variables, *Comput. Methods Appl. Mech. Eng.*, **355** (2019), 438–455. https://doi.org/10.1016/j.cma.2019.06.036
30. C. Wang, H. G. Matthies, Random model with fuzzy distribution parameters for hybrid uncertainty propagation in engineering systems, *Comput. Methods Appl. Mech. Eng.*, **359** (2020), 112673. https://doi.org/10.1016/j.cma.2019.112673
31. T. Denœux, Belief functions induced by random fuzzy sets: A general framework for representing uncertain and fuzzy evidence, *Fuzzy Sets Syst.*, **424** (2021), 63–91. https://doi.org/10.1016/j.fss.2020.12.004
32. S. Destercke, Fuzzy belief structures viewed as classical belief structures: A practical viewpoint, in *Proceedings of International Conference on Fuzzy Systems*, IEEE, (2010), 1–8. https://doi.org/10.1109/FUZZY.2010.5584668
33. D. Dubois, H. Prade, Random sets and fuzzy interval analysis, *Fuzzy Sets Syst.*, **42** (1991), 87–101. https://doi.org/10.1016/0165-0114(91)90091-4
34. T. Denœux, Extending stochastic ordering to belief functions on the real line, *Inf. Sci.*, **179** (2009), 1362–1376. https://doi.org/10.1016/j.ins.2009.01.009

35. L. A. Zadeh, Outline of a new approach to the analysis of complex systems and decision processes, *IEEE Trans. Syst. Man Cybern.*, **SMC-3** (1973), 28–44. https://doi.org/10.1109/TSMC.1973.5408575

36. H. J. Zimmermann, Fuzzy set theory, *WIREs Comput. Stat.*, **2** (2010), 317–332. https://doi.org/10.1002/wics.82

37. X. Chen, Y. He, D. Xiu, An efficient method for uncertainty propagation using fuzzy sets, *SIAM J. Sci. Comput.*, **37** (2015), A2488–A2507. https://doi.org/10.1137/140997385

38. I. R. Goodman, H. T. Nguyen, *Uncertainty Models for Knowledge-Based Systems; A Unified Approach to the Measurement of Uncertainty*, North-Holland, Amsterdam, 1985.

39. H. T. Nguyen, On random sets and belief functions, *J. Math. Anal. Appl.*, **65** (1978), 531–542. https://doi.org/10.1016/0022-247X(78)90161-0

40. R. R. Yager, Cumulative distribution functions from Dempster-Shafer belief structures, *IEEE Trans. Syst. Man Cybern.*, **34** (2004), 2080–2087. https://doi.org/10.1109/tsmcb.2004.833772

41. F. Tonon, A. Bernardini, A. Mammino, Reliability analysis of rock mass response by means of random set theory, *Reliab. Eng. Syst. Saf.*, **70** (2000), 263–282. https://doi.org/10.1016/S0951-8320(00)00059-4

42. H. Kwakernaak, Fuzzy random variables—i. definitions and theorems, *Inf. Sci.*, **15** (1978), 1–29. https://doi.org/10.1016/0020-0255(78)90019-1

43. L. A. Zadeh, Fuzzy sets and information granularity, in *Advances in Fuzzy Set Theory and Applications*, World Scientific Publishing, (1979), 3–18.

44. R. Cameron, W. Martin, The orthogonal development of nonlinear functionals in series of Fourier-Hermite functionals, *Ann. Math.*, **48** (1947), 385–392. https://doi.org/10.2307/1969178

45. R. G. Ghanem, P. D. Spanos, *Stochastic Finite Elements: A Spectral Approach*, Springer, New York, 1991. https://doi.org/10.1007/978-1-4612-3094-6

46. D. Xiu, *Numerical Methods for Stochastic Computations: A Spectral Method Approach*, Princeton University Press, New Jersey, 2010.

47. F. Heiss, V. Winschel, Likelihood approximation by numerical integration on sparse grids, *J. Econom.*, **144** (2008), 62–80. https://doi.org/10.1016/j.jeconom.2007.12.004

48. C. C. Mitchell, D. G. Schaeffer, A two-current model for the dynamics of cardiac membrane, *Bull. Math. Biol.*, **65** (2003), 767–793. https://doi.org/10.1016/S0092-8240(03)00041-7

49. J. W. Cain, D. G. Schaeffer, Two-term asymptotic approximation of a cardiac restitution curve, *SIAM Rev*, **48** (2006), 537–546. https://doi.org/10.1137/050632907

50. D. G. Schaeffer, J. W. Cain, D. J. Gauthier, S. S. Kalb, R. A. Oliver, E. G. Tolkacheva, et al., An ionically based mapping model with memory for cardiac restitution, *Bull. Math. Biol.*, **69** (2007), 459–482. https://doi.org/10.1007/s11538-006-9116-6

51. C. Sánchez, A. Bueno-Orovio, E. Wettwer, S. Loose, J. Simon, U. Ravens, et al., Inter-subject variability in human atrial action potential in sinus rhythm versus chronic atrial fibrillation, *PLoS One*, **9** (2014), e105897. https://doi.org/10.1371/journal.pone.0105897

52. J. Pearce-Lance, *Methods for Parameter Identification in the Mitchell-Schaeffer Model*, Master's thesis, University of Ottawa, 2019.

53. J. W. Cain, E. G. Tolkacheva, D. G. Schaeffer, D. J. Gauthier, Rate-dependent propagation of cardiac action potentials in a one-dimensional fiber, *Phys. Rev. E*, **70** (2004), 061906. https://doi.org/10.1103/PhysRevE.70.061906

54. M. Reidenbach, N. George, M. Koehl, Antennule morphology and flicking kinematics facilitate odor sampling by the spiny lobster, *Panulirus argus*, *J. Exp. Biol.*, **211** (2008), 2849–2858. https://doi.org/10.1242/jeb.016394

55. L. Waldrop, M. Reidenbach, M. Koehl, Flexibility of crab chemosensory sensilla enables flicking antennules to sniff, *Biol. Bull.*, **229** (2015), 185–198. https://doi.org/10.1086/BBLv229n2p185

56. B. E. Griffith, S. Lim, Simulating an elastic ring with bend and twist by an adaptive generalized immersed boundary method, *Commun. Comput. Phys.*, **12** (2012), 433–461. https://doi.org/10.4208/cicp.190211.060811s

57. B. E. Griffith, X. Luo, Hybrid finite difference/finite element immersed boundary method, *Int. J. Numer. Methods Biomed. Eng.*, **33** (2017), e2888. https://doi.org/10.1002/cnm.2888

58. L. Waldrop, Y. He, S. Khatri, What can computational modeling tell us about the diversity of odor-capture structures in the pancrustacea?, *J. Chem. Ecol.*, **44** (2018), 1084–1100. https://doi.org/10.1007/s10886-018-1017-2

59. L. Waldrop, Ontogenetic scaling of the olfactory antennae and flicking behavior of the shore crab, *Hemigrapsus oregonensis*, *Chem. Senses*, **38** (2013), 541–550. https://doi.org/10.1093/chemse/bjt024

60. L. Waldrop, R. Bantay, Q. Nguyen, Scaling of olfactory antennae of the terrestrial hermit crabs *Coenobita rugosus* and *Coenobita perlatus* during ontogeny, *PeerJ*, **2** (2014), e535. https://doi.org/10.7717/peerj.535

61. R. Gleeson, Pheromone communication in the reproductive behavior of the blue crab, *Callinectes sapidus*, *Mar. Behav. Physiol.*, **7** (1980), 119–134. https://doi.org/10.1080/10236248009386976

62. R. Gleeson, L. McDowell, H. Aldrich, Structure of the aesthetasc (olfactory) sensilla of the blue crab, *Callinectes sapidus*: Transformations as a function of salinity, *Cell Tissue Res.*, **284** (1996), 279–288. https://doi.org/10.1007/s004410050588

63. J. Goldman, M. Koehl, Fluid dynamic design of lobster olfactory organs: High speed kinematic analysis of antennule flicking by *Panulirus argus*, *Chem. Senses*, **26** (2001), 385–398. https://doi.org/10.1093/chemse/26.4.385

64. J. Goldman, S. Patek, Two sniffing strategies in palinurid lobsters, *J. Exp. Biol.*, **205** (2002), 3891–3902. https://doi.org/10.1242/jeb.205.24.3891

65. D. Weisbaum, K. Lavalli, Morphology and distribution of antennular setae of scyllarid lobsters (*Scyllarides aequinoctialis*, *S. latus*, and *S. nodifer*) with comments on their possible function, *Invertebr. Biol.*, **123** (2004), 324–342. https://doi.org/10.1111/j.1744-7410.2004.tb00166.x

66. K. Mead, Do antennule and aesthetasc structure in the crayfish *Orconectes virilis* correlate with flow habitat?, *Integr. Comp. Biol.*, **48** (2008), 823–833. https://doi.org/10.1093/icb/icn067

67. S. Pravin, D. Mellon, M. Reidenbach, Micro-scale fluid and odorant transport to antennules of the crayfish, *Procambarus clarkii*, *J. Comp. Physiol. A*, **198** (2012), 669–681. https://doi.org/10.1007/s00359-012-0738-x

68. J. Nelson, D. Mellon, M. Reidenbach, Effects of antennule morphology and flicking kinematics on flow and odor sampling by the freshwater crayfish, *Procambarus clarkii*, *Chem. Senses*, **38** (2013), 729–741. https://doi.org/10.1093/chemse/bjt041

69. H. Monteclaro, K. Anraku, T. Matsuoka, Response properties of crayfish antennules to hydrodynamic stimuli: functional differences in the lateral and medial flagella, *J. Exp. Biol.*, **213** (2010), 3683–3691. https://doi.org/10.1242/jeb.046011

70. A. Cheer, M. Koehl, Paddles and rakes: Fluid flow through bristled appendages of small organisms, *J. Theor. Biol.*, **129** (1987), 17–39. https://doi.org/10.1016/S0022-5193(87)80201-1

71. C. Loudon, M. Koehl, Sniffing by a silkworm moth: Wing fanning enhances air penetration through and pheromone interception by antennae, *J. Exp. Biol.*, **203** (2000), 2977–2990. https://doi.org/10.1242/jeb.203.19.2977

72. K. Mead, M. Koehl, M. O'Donnell, Stomatopod sniffing: The scaling of chemosensory sensillae and flicking behavior with body size, *J. Exp. Mar. Biol. Ecol.*, **241** (1999), 235–261. https://doi.org/10.1016/S0022-0981(99)00087-8

73. K. Mead, M. Koehl, Stomatopod antennule design: The asymmetry, sampling efficiency and ontogeny of olfactory flicking, *J. Exp. Biol.*, **203** (2000), 3795–3808. https://doi.org/10.1242/jeb.203.24.3795

74. H. Childs, E. Brugger, B. Whitlock, J. Meredith, S. Ahern, D. Pugmire, et al., VisIt: An end-user tool For visualizing and analyzing very large data, in *High Performance Visualization–Enabling Extreme-Scale Scientific Insight*, Chapman and Hall/CRC, (2012), 357–372.

75. R. D. C. Team, R Foundation for Statistical Computing, Vienna, Austria, 2011. Available from: http://www.r-project.org.

76. T. Hastie, R. Tibshirani, J. Friedman, *The Elements of Statistical Learning: Data Mining, Inference, and Prediction, Second Edition*, Springer, New York, 2009. https://doi.org/10.1007/978-0-387-84858-7

AIMS Press